Beam Dynamics in Insertion Devices

- Closed orbit perturbation and correction
- Linear optics perturbation and correction
- Nonlinear dynamics
  - After sextupoles, IDs are the biggest nonlinearity at light sources and damping rings
  - Nonlinearities from construction tolerances
  - Nonlinearities intrinsic to insertion device design
    - Linearly polarized ID
    - End correctors
    - Elliptically polarized ID

What is an insertion device?

- An insertion device has a periodic magnetic field designed to make the electron trajectory wiggle and generate intense synchrotron radiation.
- Wiggler and undulator IDs generate different synchrotron radiation spectra, but are essentially the same as far as beam dynamics are concerned. Undulators tend to have shorter periods and weaker fields.
- Used as synchrotron radiation sources, in storage ring colliders and in damping rings for linear colliders.

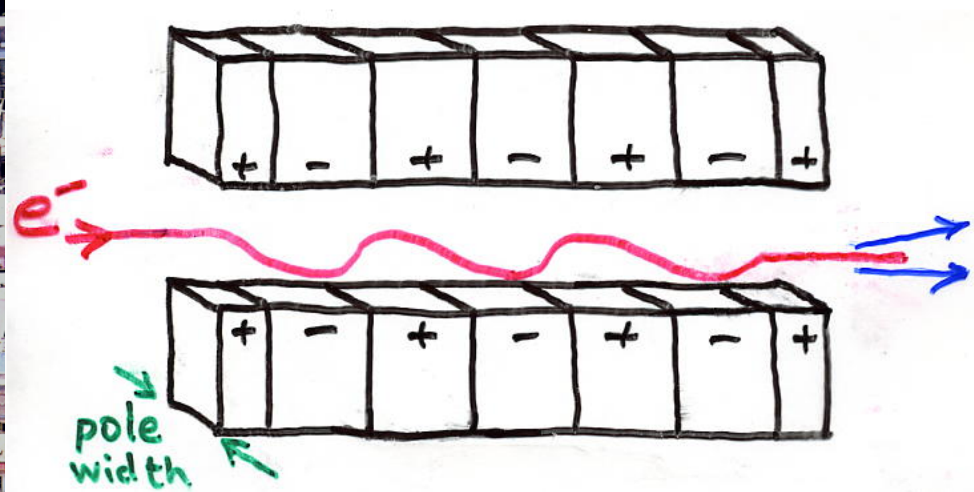

First Wiggler Magnet,1978, SSRL

Bending Magnets, Wigglers and Undulators

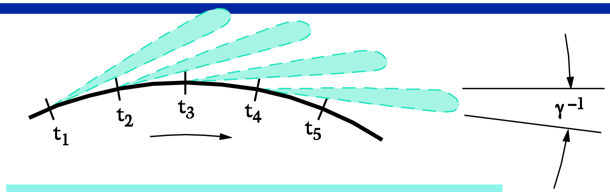

bending magnet - a "sweeping searchlight"

Continuous spectrum characterized by ε_c = critical energy

$$\varepsilon_c(\text{keV}) = 0.665\ B(\text{T})E^2(\text{GeV})$$

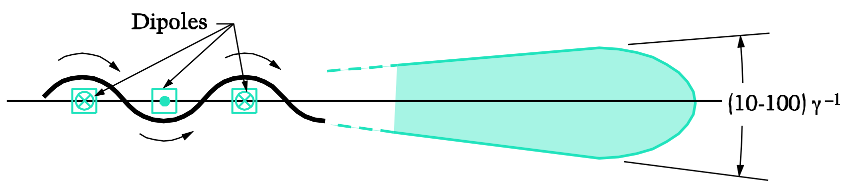

wiggler - incoherent superposition

Intensity ~ N_{poles}

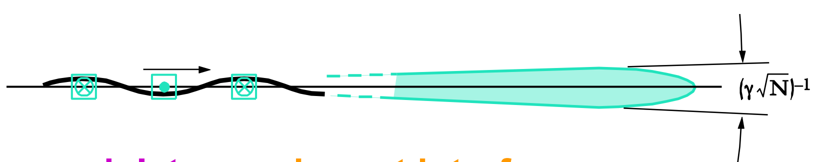

undulator - coherent interference

Quasi-monochromatic spectrum with peaks at lower energy than a wiggler

$$\lambda_1 = \frac{\lambda_u}{2\gamma^2}\left(1 + \frac{K^2}{2}\right) \sim \frac{\lambda_U}{\gamma^2} \text{ (fundamental)}$$

+ harmonics at higher energy

$$\varepsilon_1 (\text{keV}) = \frac{0.95\ E^2\ (\text{GeV})}{\lambda_u{}^{(\text{cm})}\left(1 + \frac{K^2}{2}\right)}$$

$K = \gamma\theta$ where θ is the angle in each pole

Planar Undulators

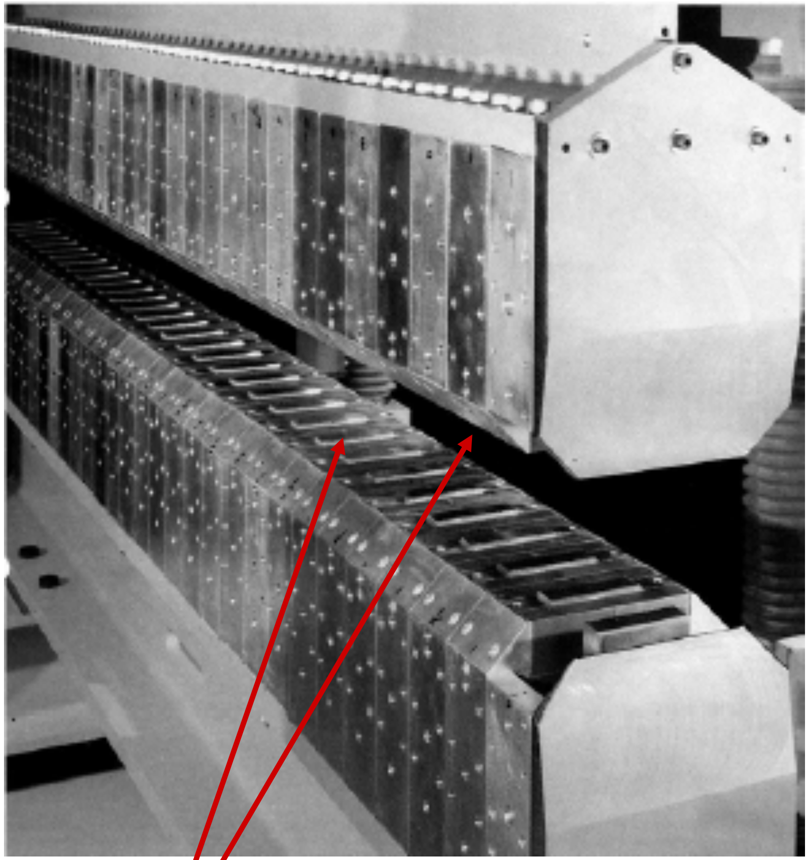

Permanent Magnets

Invented by
Klaus Halbach

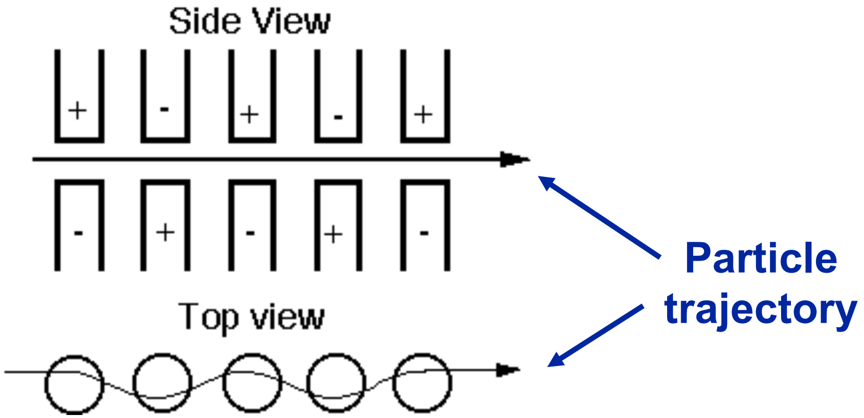

Undulator radiation

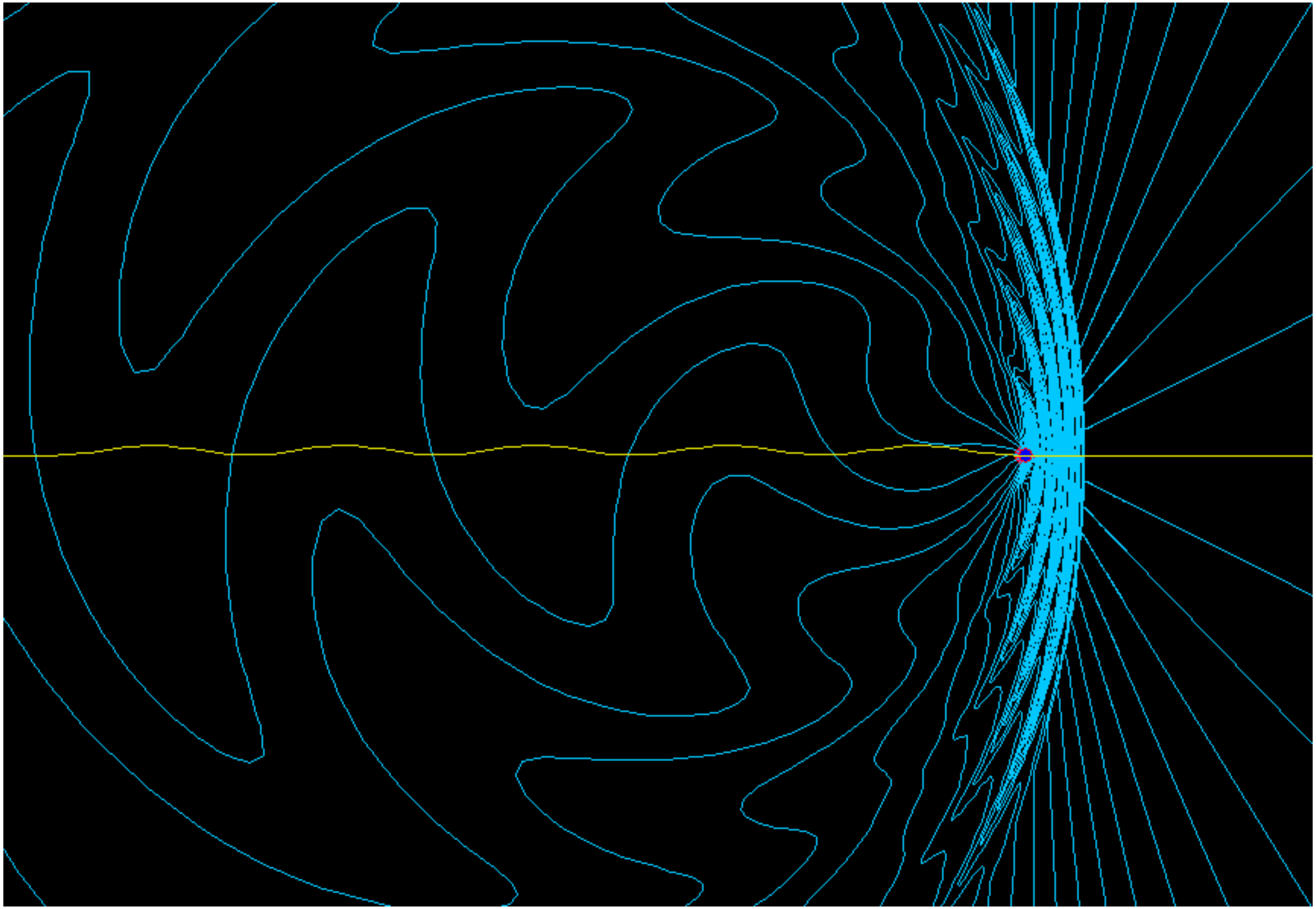

Insertion device examples

•Can be made of permanent magnets, electromagnets, or superconducting.

• Can be linearly polarized, so electrons wiggle in one plane, or elliptically polarized, so electrons travel in elliptical helixes generating elliptically polarized γs.

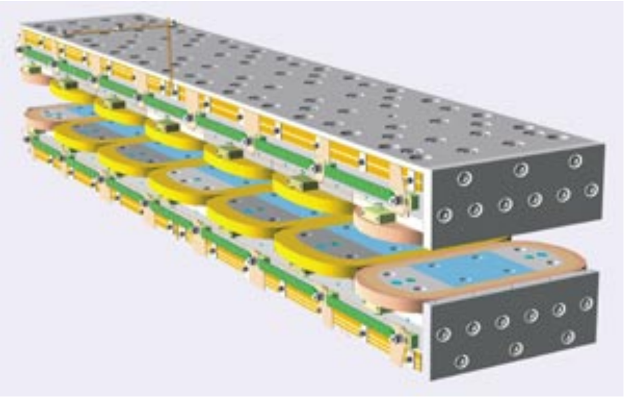

CESR superferric wiggler

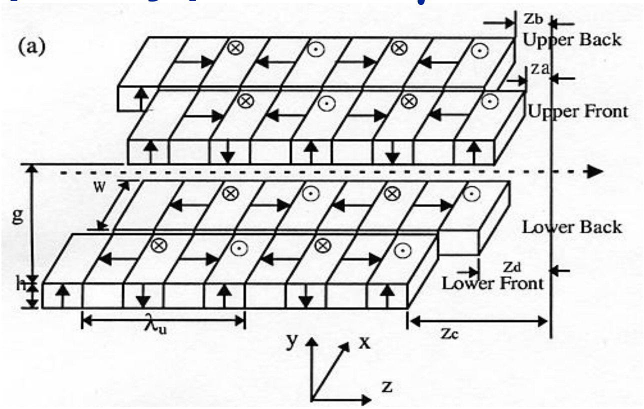

Variable elliptical polarization

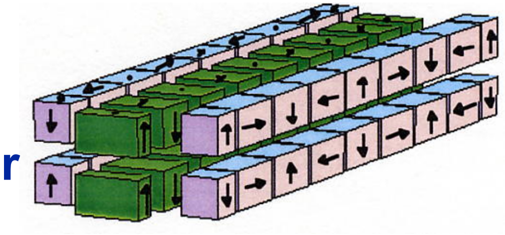

Figure 8 undulator

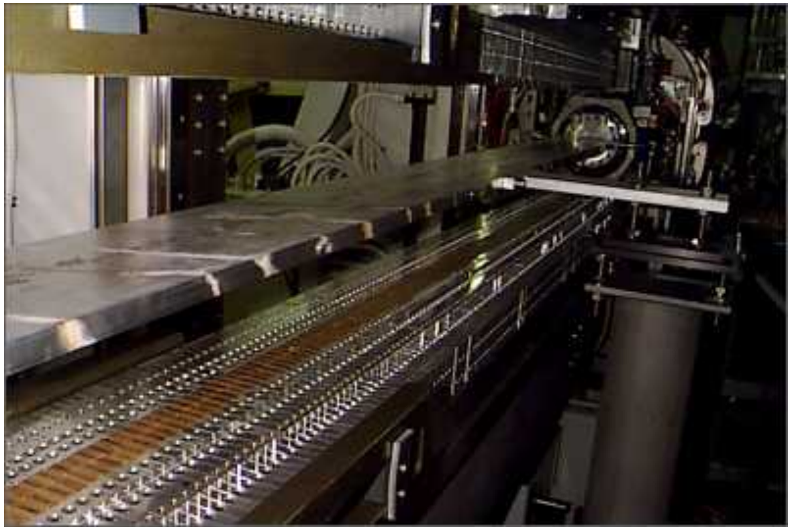

Elettra permanent magnet ID

Control of closed orbit

Often users adjust the spectrum from undulators by changing undulator gaps or row phase in EPUs. It's important to keep the orbit constant during these field changes to not disrupt other users. Usually use two steering magnets to correct the first and second field integrals.

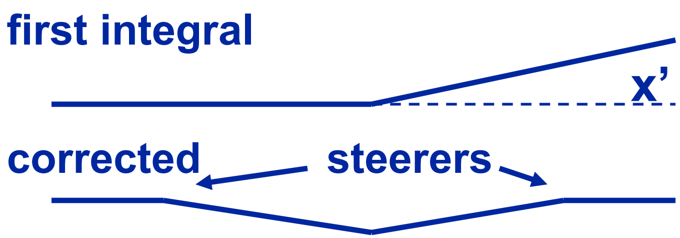

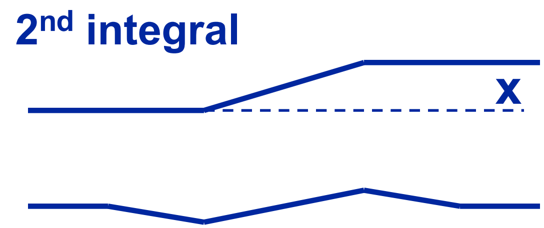

Example: EPW at NSLS switches at 100 Hz (Singh and Krinsky, PAC'97)

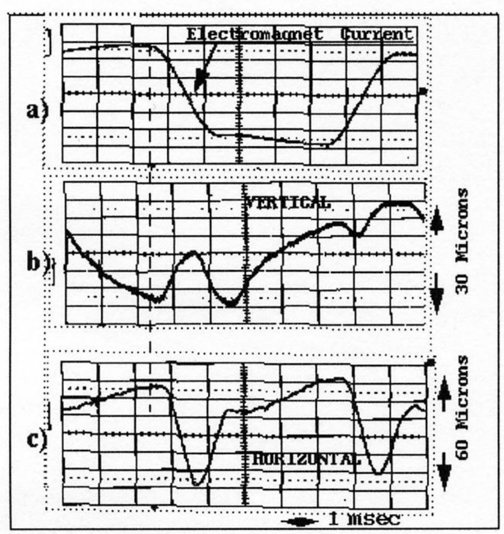

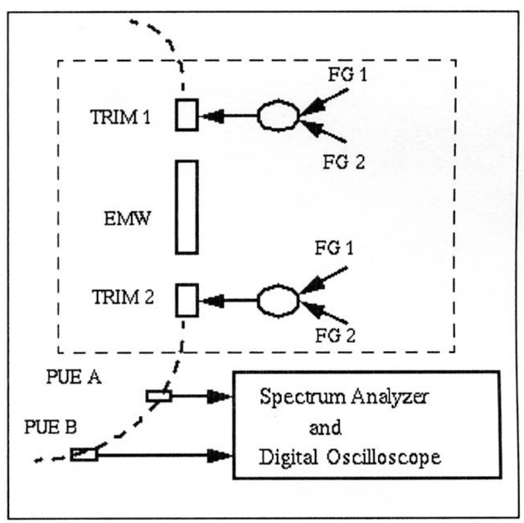

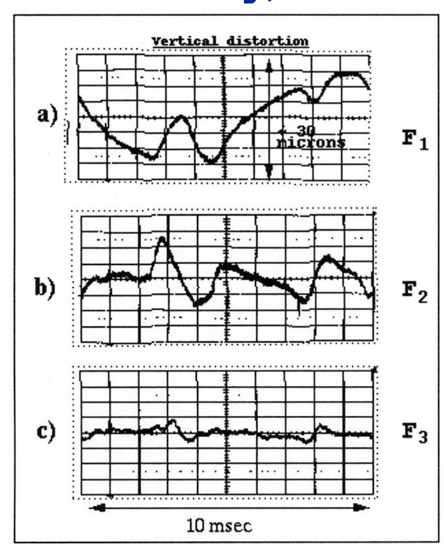

Elliptically Polarizing Undulator (EPU)

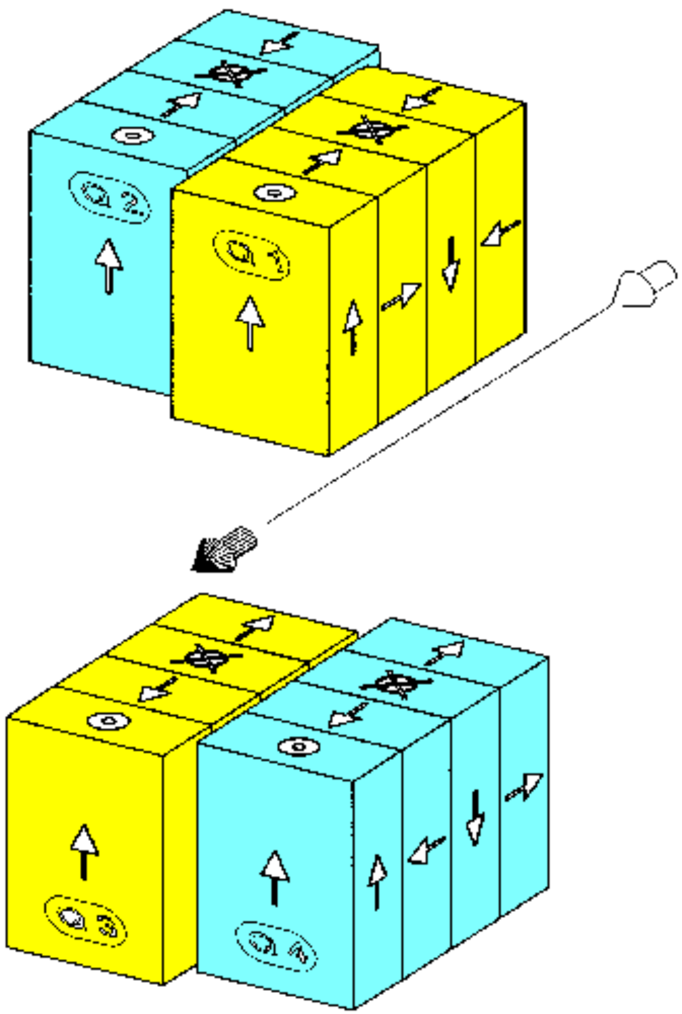

The EPU is different than other insertion devices

- The jaws can move in two directions

  (vertically and longitudinally)

- The motion in the longitudinal direction is fast

  (At the ALS, up to 17 mm/second)

This makes ***orbit compensation*** *more difficult than other insertion devices*

Feed-forward example: EPU

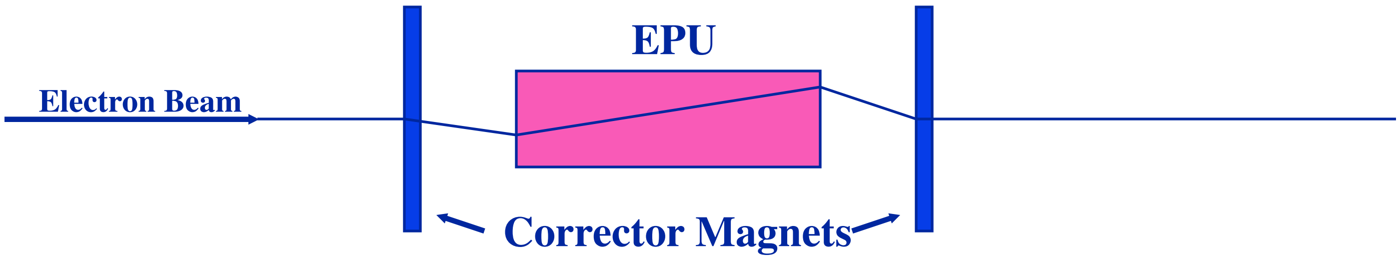

Mechanically, an ALS EPU can move from left to right circular polarization mode in ~1 sec.

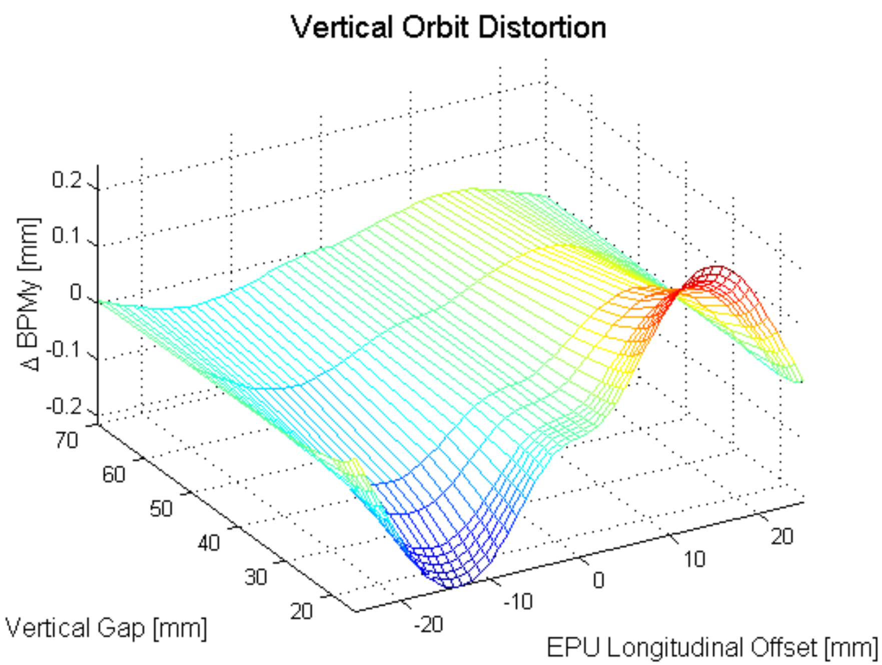

Without compensation the EPU would distort the electron beam orbit by ±200 μm vertically and ±100 μm horizontally. Using corrector magnets on either side of the EPU, 2-dimensional feed forward correction tables are used to reduce the orbit distortion to the 2-3 μm level. Update rate of feed-forward is 200 Hz.

Feed-forward tables based on beam based measurements are much more accurate than ones based on magnetic bench measurements.

For even faster switching devices (CPW, …) eddy current effects make beam based optimization even more important.

EPU FEED FORWARD ORBIT CORRECTION at ALS

Orbit Error without Feed Forward Correction

100 Hz Feed Forward Correction

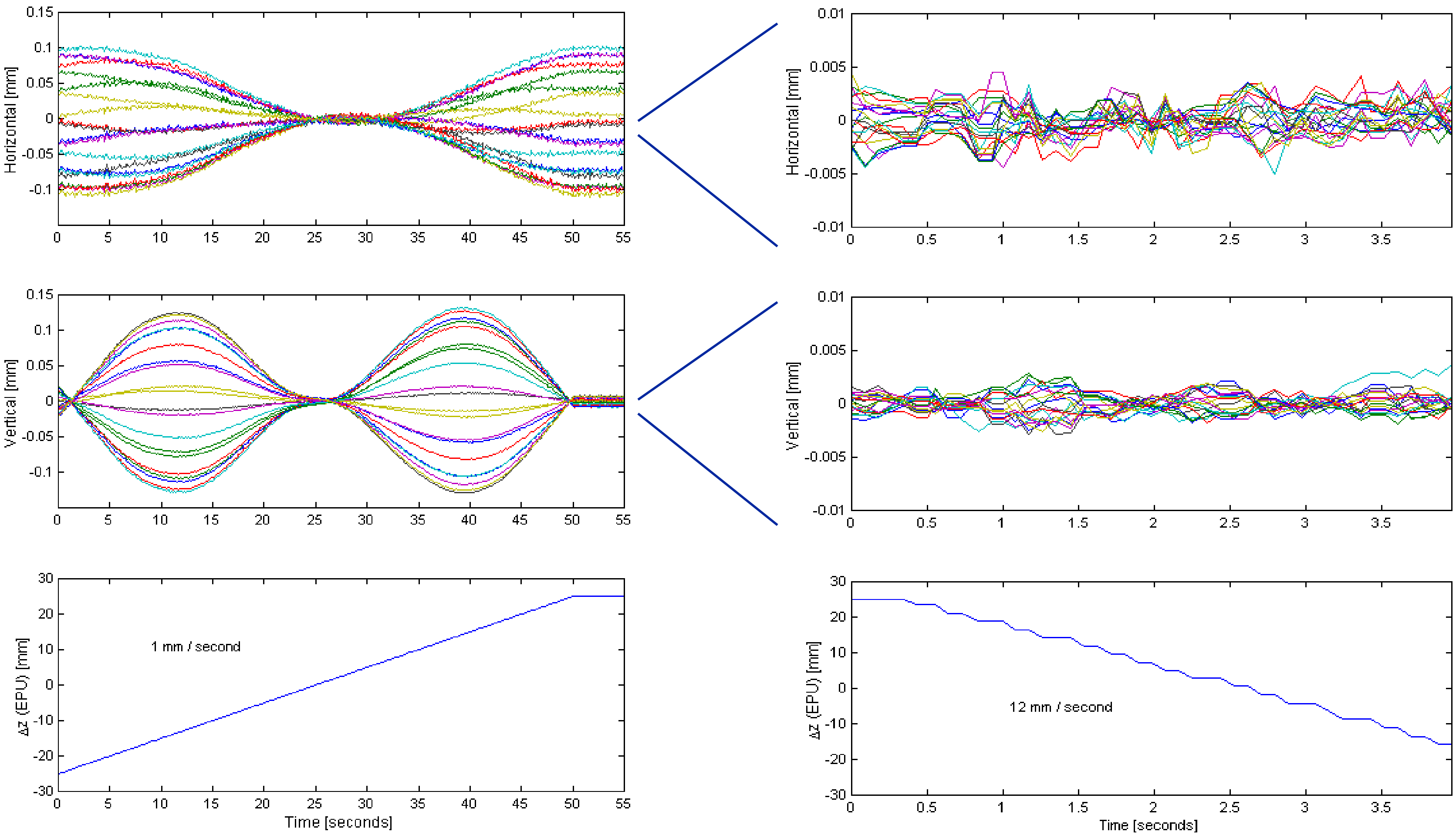

Implemented since 2000

C. Steier

Fields in insertion devices

The fields in wigglers must satisfy Maxwell's equations in free space:

$$\vec{B} = \nabla \Phi_B \qquad (\Rightarrow \nabla \times \vec{B} = 0)$$

$$\nabla^2 \Phi_B = 0 \qquad (\, from \; \nabla \cdot \vec{B} = 0)$$

The ID is periodic in z, so let $\Phi_B = f(x, y) \cos kz$

A real ID has higher longitudinal harmonics, $\sim \cos nkz \, , n = 1,3,5 \ldots$
but the simpler model is good enough for now.

$$\nabla^2 \Phi_B = 0 \quad \Rightarrow \quad \frac{\partial^2 f}{\partial x^2} + \frac{\partial^2 f}{\partial y^2} = k^2 f$$

A solution is

$$f = \frac{B_0}{k_y} \cos(k_x x) \sinh(k_y y)$$

$$-k_x{}^2 + k_y{}^2 = k^2$$

The reason to choose this particular solution is …

Fields in insertion devices, II

The resulting magnetic fields are

$$B_y = B_0 \cos(k_x x)\cosh(k_y y)\cos(kz)$$

$$B_x = -\frac{k_x}{k_y} B_0 \sin(k_x x)\sinh(k_y y)\cos(kz)$$

$$B_z = -\frac{k}{k_y} B_0 \cos(k_x x)\sinh(k_y y)\sin(kz)$$

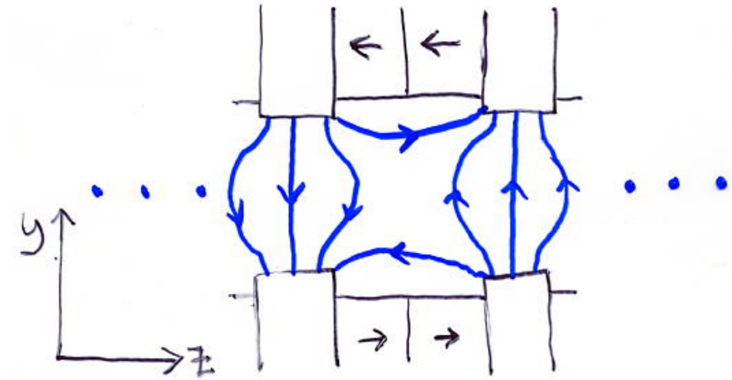

This gives B_y dropping off with x, which is the case with most IDs, due to finite magnet pole width. It gives B_y increasing with y, approaching the magnet poles.

These fields provide a basis for describing a real linearly polarized ID. A real ID has higher harmonic components in z. In x, there is no constraint on k_x, so in general the fields can be described with a Fourier transform of the roll-off of B_y with x, with $k_y^2=k^2+k_x^2$ for each Fourier component.

Linear optics in IDs

IDs generate vertical focusing from the wiggling electron trajectory crossing B_z at an angle between the poles. This is like the vertical focusing in the end fields of a rectangular dipole magnet.

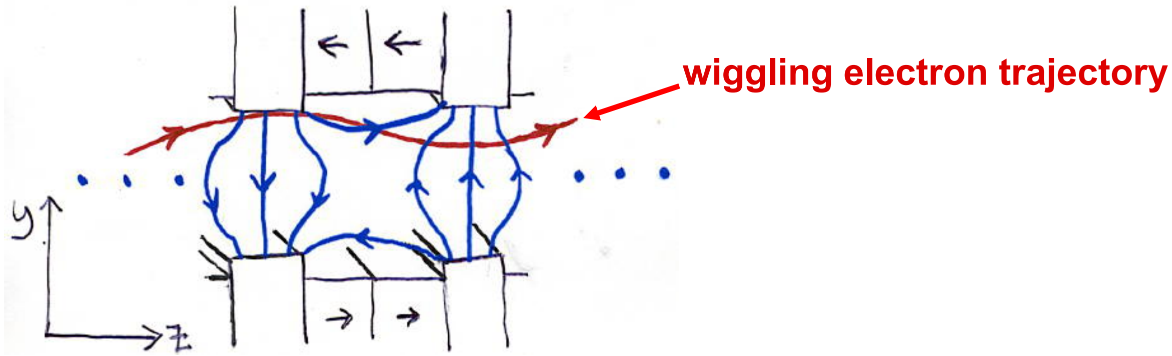

IDs generate horizontal defocusing (and further vertical focusing) from the wiggling electron trajectory sampling the gradient of the roll off of B_y with x.

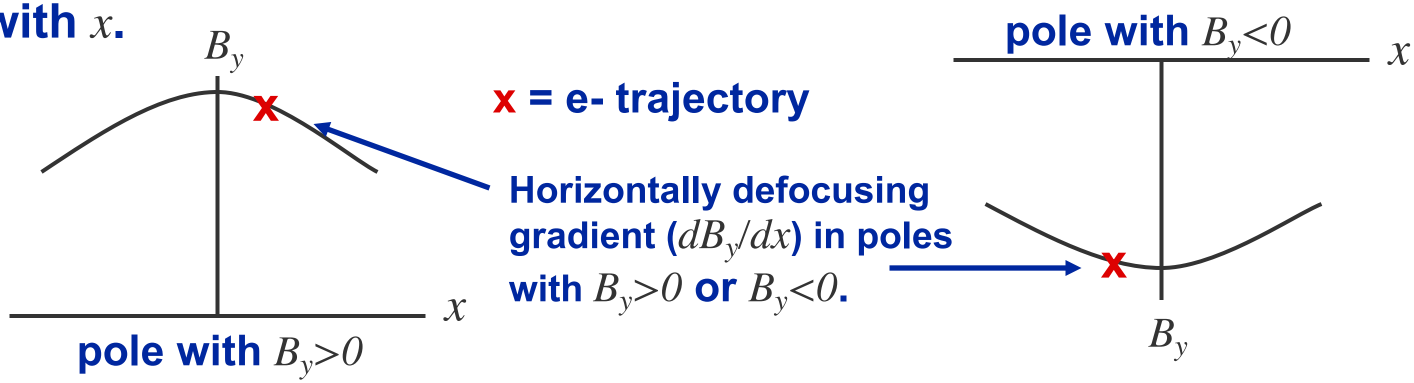

Linear optics in IDs, II

The linear equations of motion in the wiggler fields expanded about the wiggling trajectory are[1]:

$$x'' = \frac{1}{2\rho^2}\frac{k_x^2}{k^2}x \qquad y'' = -\frac{1}{2\rho^2}\frac{k_y^2}{k^2}y$$

This linear optics perturbation causes:

1. Breaking the design periodicity of a storage ring. This can lead to degradation of the dynamic aperture.

2. Variation in beam sizes around the ring when users are changing their ID gaps. The variations can come from β function variations or coupling perturbations from skew gradients in the IDs.

The optics are corrected by adjusting quadrupoles in the vicinity of the ID as a function of the ID gap.

1.) L. Smith, LBNL, ESG Technical Note No. 24, 1986.

Linear optics correction

The code LOCO can be used in a beam-based algorithm for correcting the linear optics distortion from IDs with the following procedure:

1. Measure the response matrix with the ID gap open.
2. Then the response matrix is measured with the gap closed.
3. Fit the first response matrix to find a model of the optics without the ID distortion.
4. Starting from this model, LOCO is used to fit a model of the optics including the ID. In this second fit, only a select set of quadrupoles in the vicinity of the ID are varied. The change in the quadrupole gradients between the 1^{rst} and 2nd fit models gives a good correction for the ID optics distortion.
5. Alternatively, LOCO can be used to accurately fit the gradient perturbation from the ID, and the best correction can be calculated in an optics modeling code.

1.) L. Smith, LBNL, ESG Technical Note No. 24, 1986.

Linear optics correction at ALS

Beta function distortion from wiggler.

At ALS the quadrupoles closest to the IDs are not at the proper phase to correct optics distortions, so the optics correction cannot be made entirely local.

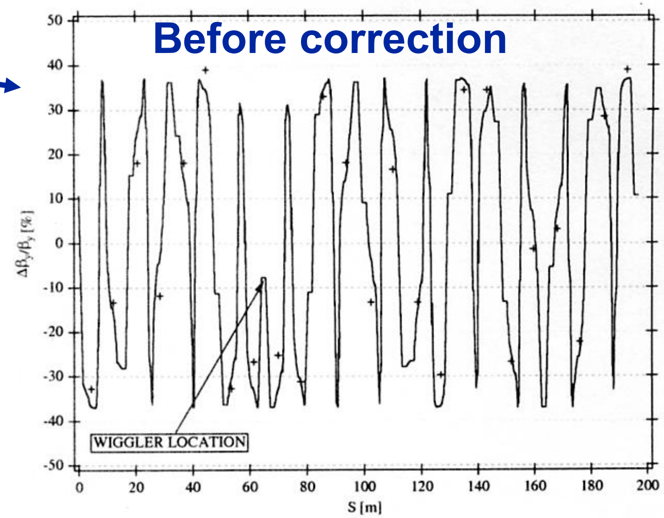

Quadrupole changes used for correction

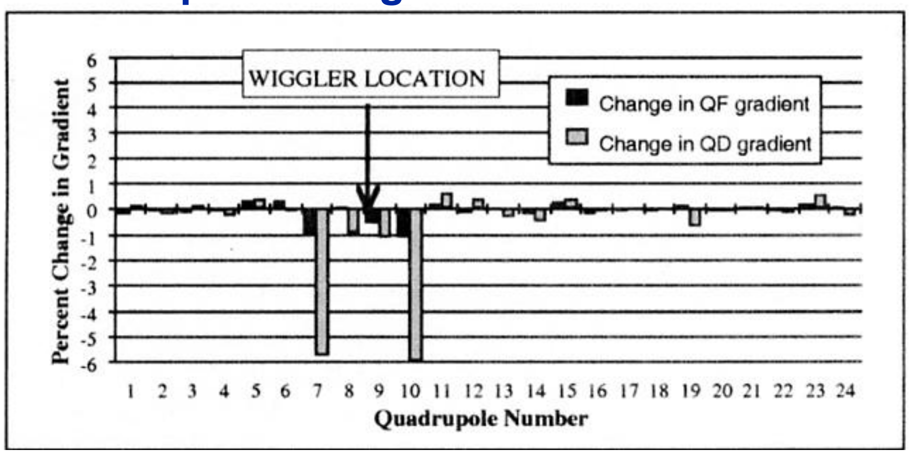

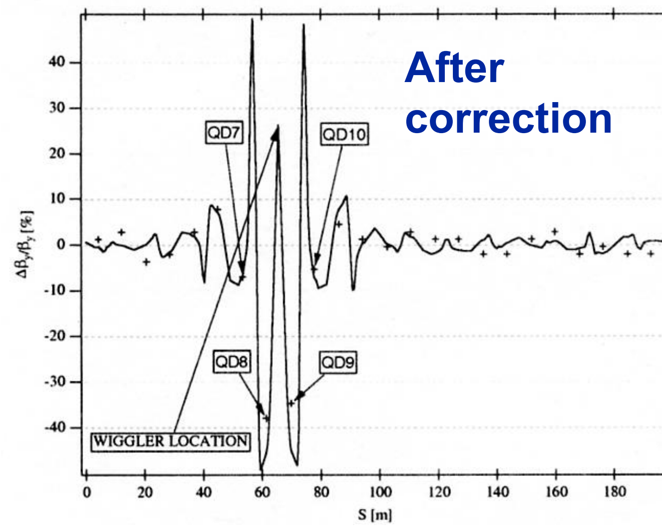

D. Robin et al. PAC97

Optics correction at SPEAR3

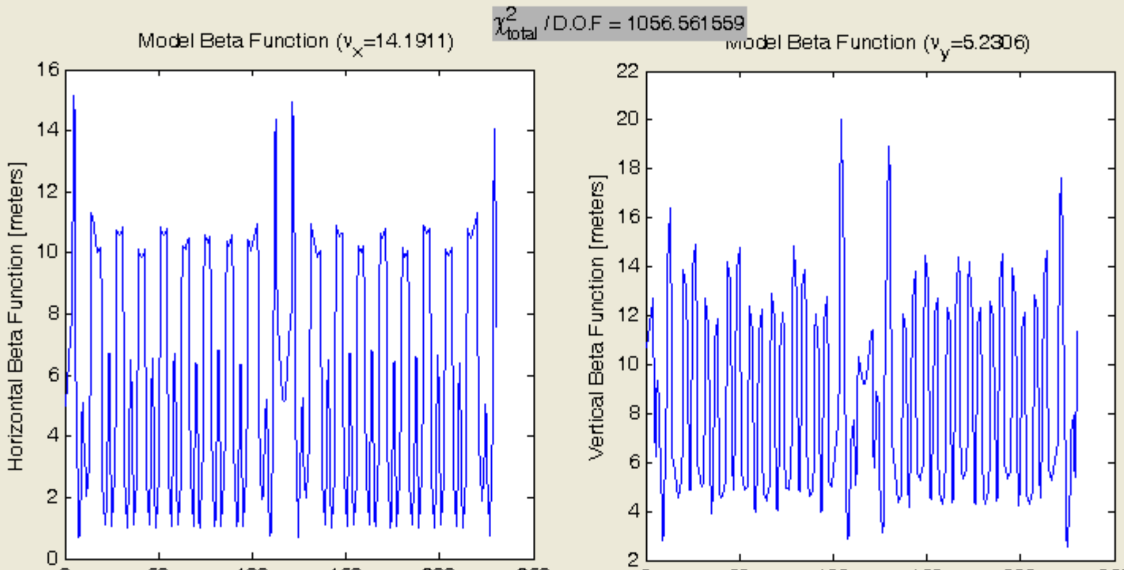

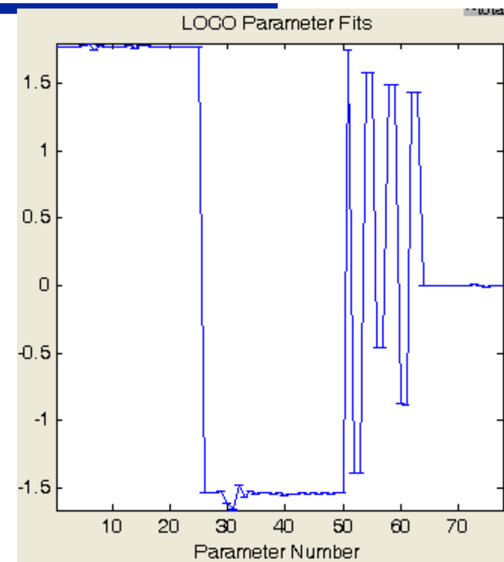

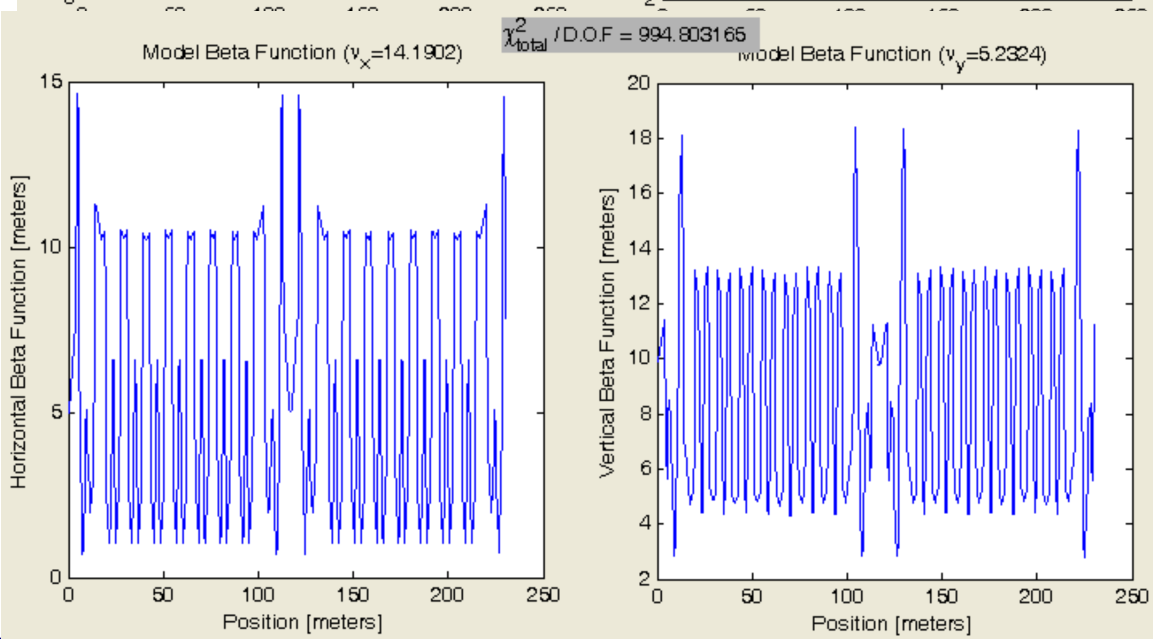

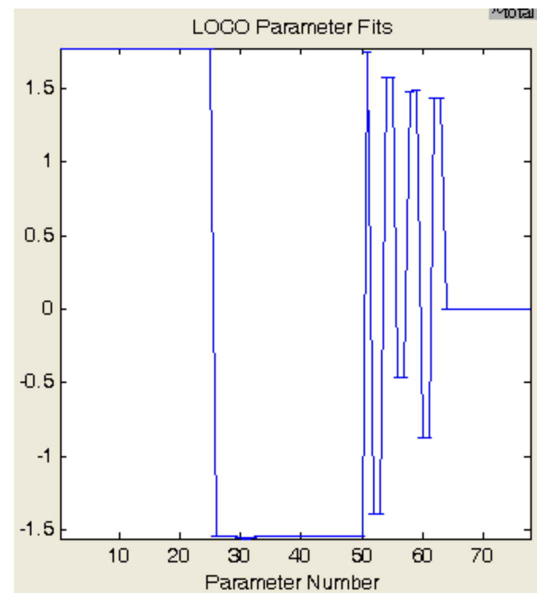

Skew quadrupole compensation for ALS EPUs

- Beamsize variation was solved in 2004: Installed correction coils for feedforward based compensation – routine use since June/September
- Early 2005 we identified the root cause: 2-3 micron correlated motion of magnet modules due to magnetic forces
- Will be able to modify design of future device such that active correction will not be necessary!

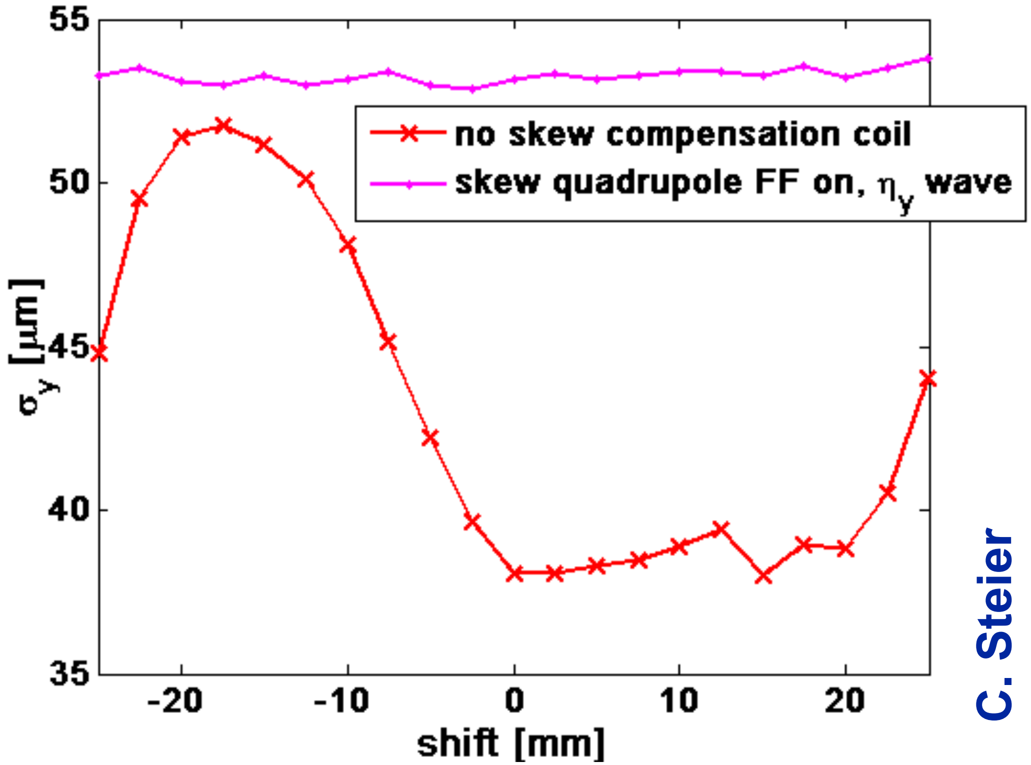

C. Steier

- Just for reference: Whenever an undulator moves, about 120-150 magnets are changed to compensate for the effect (slow+fast feed-forward, slow+fast feedback)

Nonlinear dynamics, construction tolerances & static field integrals

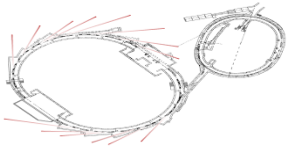

Example of nonlinear fields from construction tolerances, beamline 9 wiggler at SSRL:

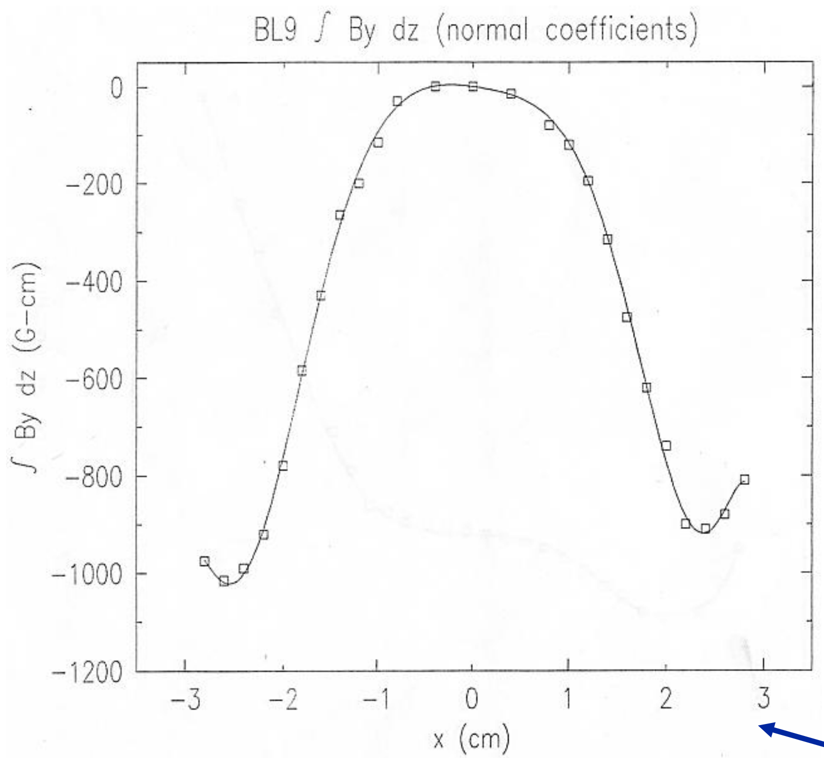

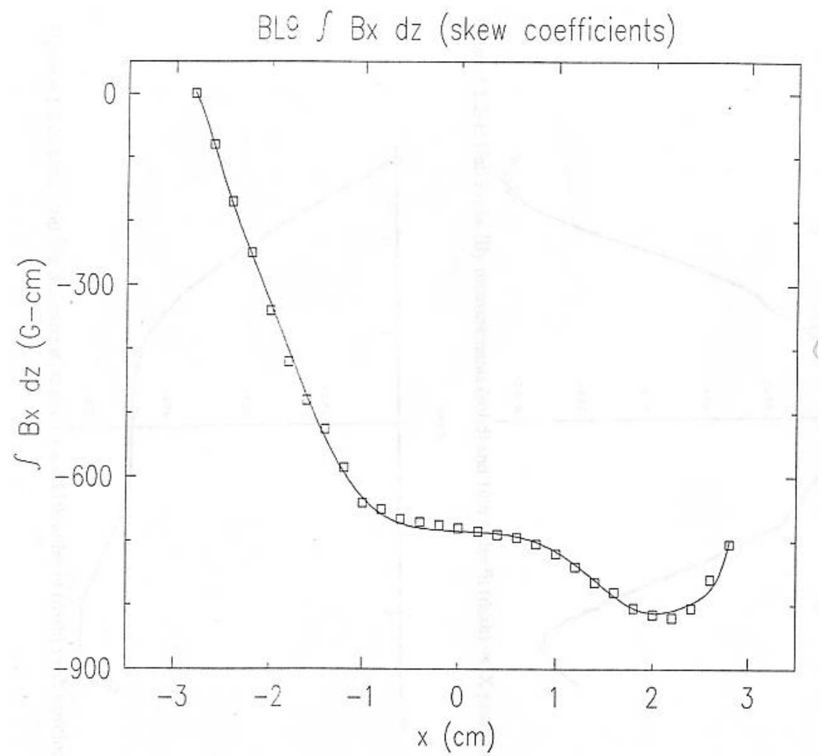

Taylor series fit to magnetic measurements gives normal and skew multipoles.

Beam-based characterization of BL9 field integrals

Measurement of tune with closed orbit bump:

$$\Delta\nu_x(x_{c.o.}) = \frac{\beta_x}{4\pi}\Delta(KL) = \frac{\beta_x}{4\pi B\rho}\frac{\partial}{\partial x}\int B_y dz$$

Closed orbit, $x_{c.o}$, varied with a 4-magnet bump. To avoid systematic errors, standardize bump magnets and correct bump coefficients for ID linear focusing and/or use feedback to generate closed bump.

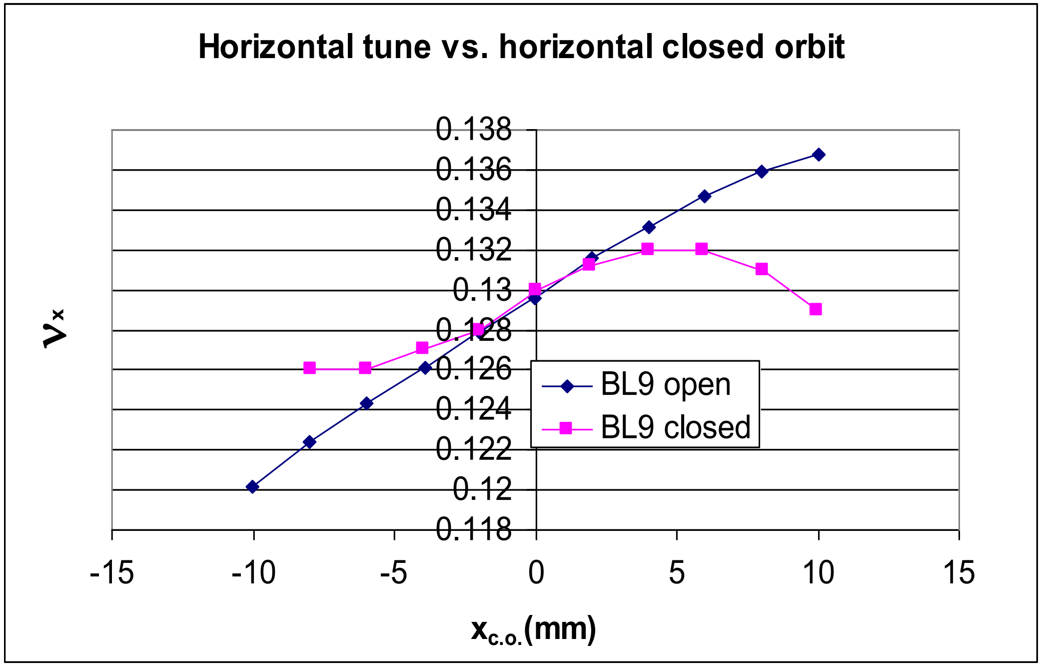

Beam-based characterization of BL9 normal multipoles

The field integral derivative according to the measured tune shift can be compared to the field integral derivative from magnetic measurements:

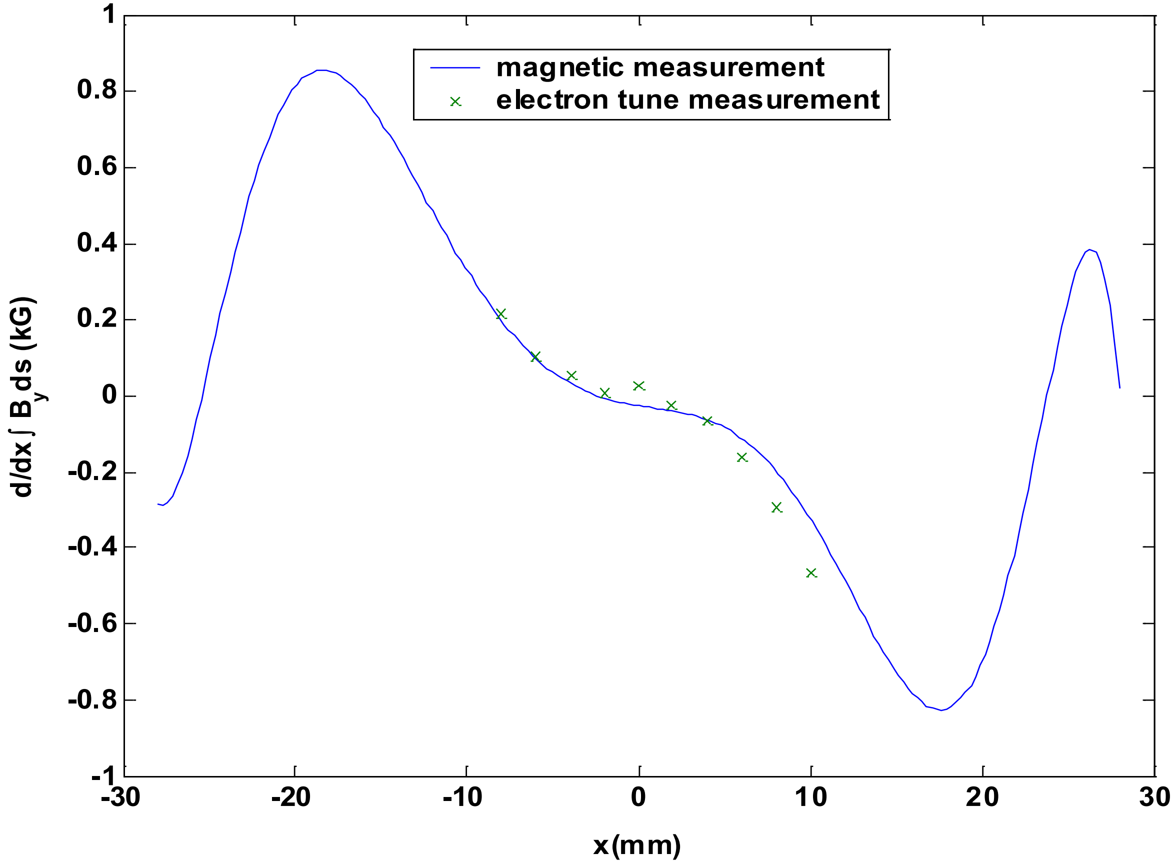

Measurement could not extend beyond +/-10 mm, for fear of melting vacuum chamber.

Beam-based method was successful in characterizing normal multipoles.

Beam-based characterization of skew multipoles

For the normal multipoles, we used tune shifts from normal gradient as a beam-based diagnostic. For skew multipoles, the skew gradient does not give such a straightforward signature as tune. Instead, the vertical orbit shift (integrated field rather than integrated gradient) can be a beam-based diagnostic.

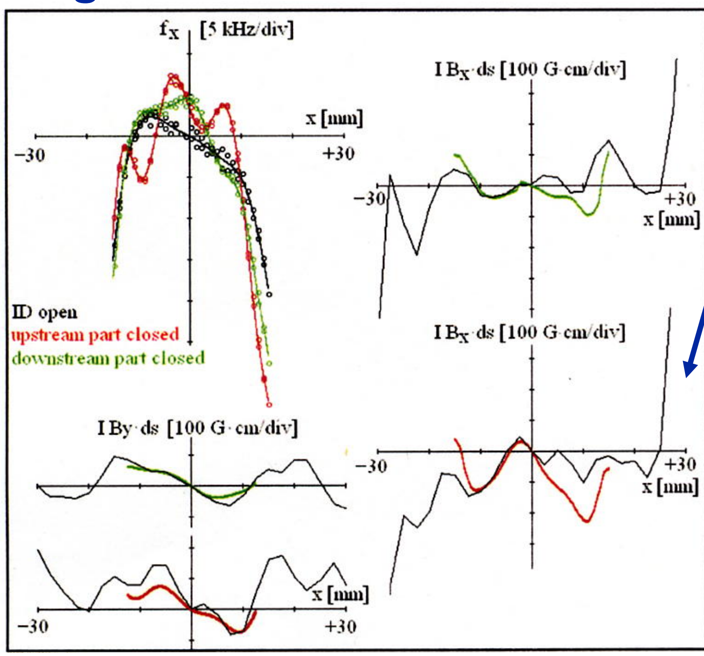

This gave reasonable results at BESSY (Kuske et al.)

Not such good results at SSRL.

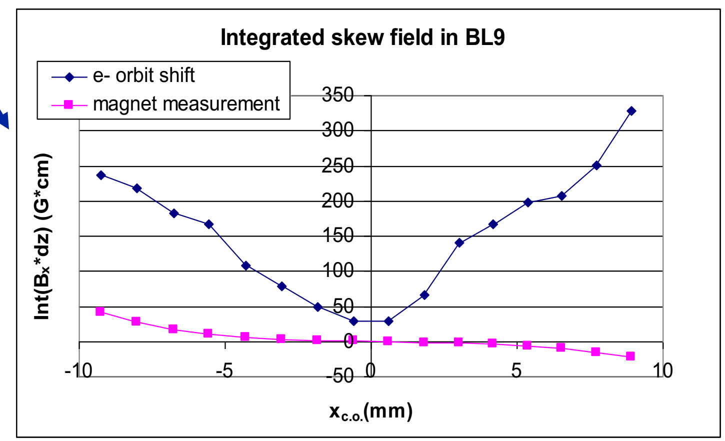

?

Beam-based characterization of skew multipoles

For the normal multipoles, we used tune shifts from normal gradient as a beam-based diagnostic. For skew multipoles, the skew gradient does not give such a straightforward signature as tune. Instead, the vertical orbit shift (integrated field rather than integrated gradient) can be a beam-based diagnostic.

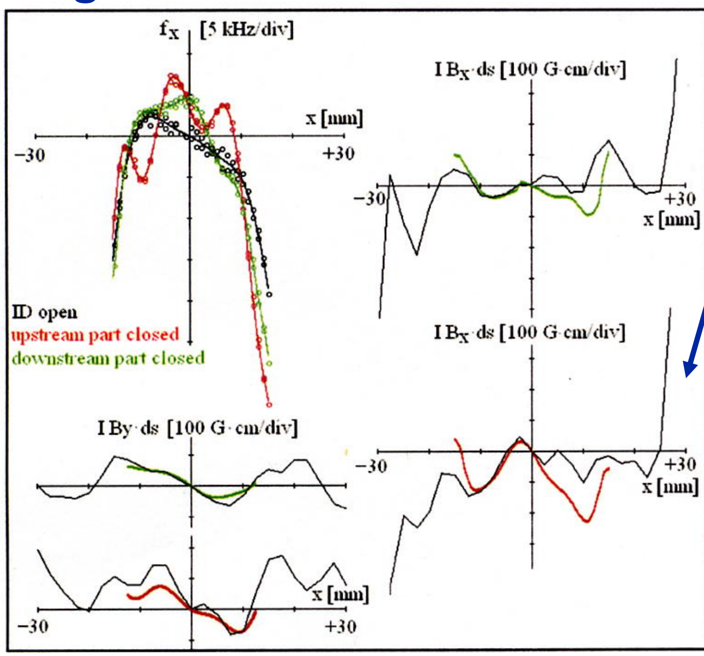

This gave reasonable results at BESSY (Kuske et al.)

Not such good results at SSRL.

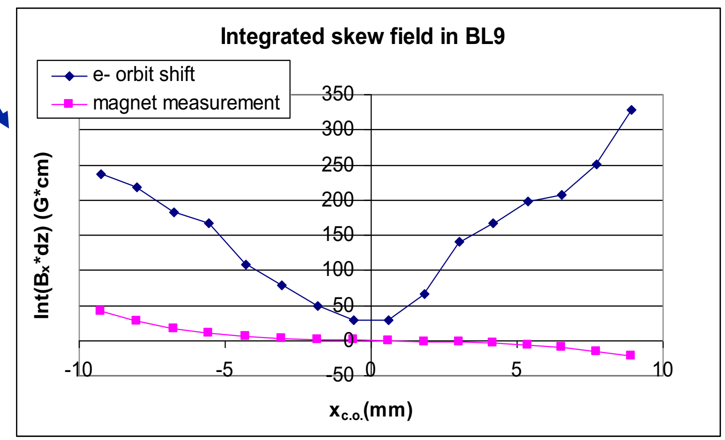

Applying LOCO to a series of orbit response matrices measured for varying closed orbit in an ID would probably give a better beam-based calibration of skew multipoles.

SSRL ID field integral specifications

- On-axis (x=y=0) specifications, normal, b_n, and skew, a_n
  - Integrated quadrupole < 50 G
  - Integrated sextupole < 75 G/cm
  - Integrated octupole < 40 G/cm^2

$$\int (B_x - iB_y)dz = \sum (a_n + ib_n)(x+iy)^n$$

- Off-axis specifications
  - 1st integral of B_y < 100 + 50*|x| G*cm, |x|<2.5 cm
  - 1st integral of B_x < 40 + 75*|x| G*cm, |x|<2.5 cm
  - 2nd integral of B_y < 1.5e4+1e4*|x| G*cm^2, |x|<2.5 cm.
  - 2nd integral of B_x < 5e3+1e4*|x| G*cm^2, |x|<2.5 cm
  - 1st integral deriv. < 50+150*|x| G; |x|<2.5 cm, $\frac{\partial}{\partial x}\int B_{x,y}dz$
- Peak field transverse roll-off
  - dB_y/dx < 11000+5500*|x| G/cm, |x|<2.5 cm (BL12)
  - dB_y/dx < 870+440*|x| G/cm, |x|<2.5 cm (BL13)
  - d^2B_y/dx^2 < 15000+20000*|x| G/cm^2, |x|<2.5 cm (BL12)
  - d^2B_y/dx^2 < 1200+1500*|x| G/cm^2, |x|<2.5 cm (BL13)
- Accelerator physics group will review fields, once the ID is designed.
- Accelerator physics group will review magnetic measurements plan.

Controls static (construction tolerance) field integrals

Controls dynamic field integrals (intrinsic to magnet design)

First integral field specifications at different laboratories

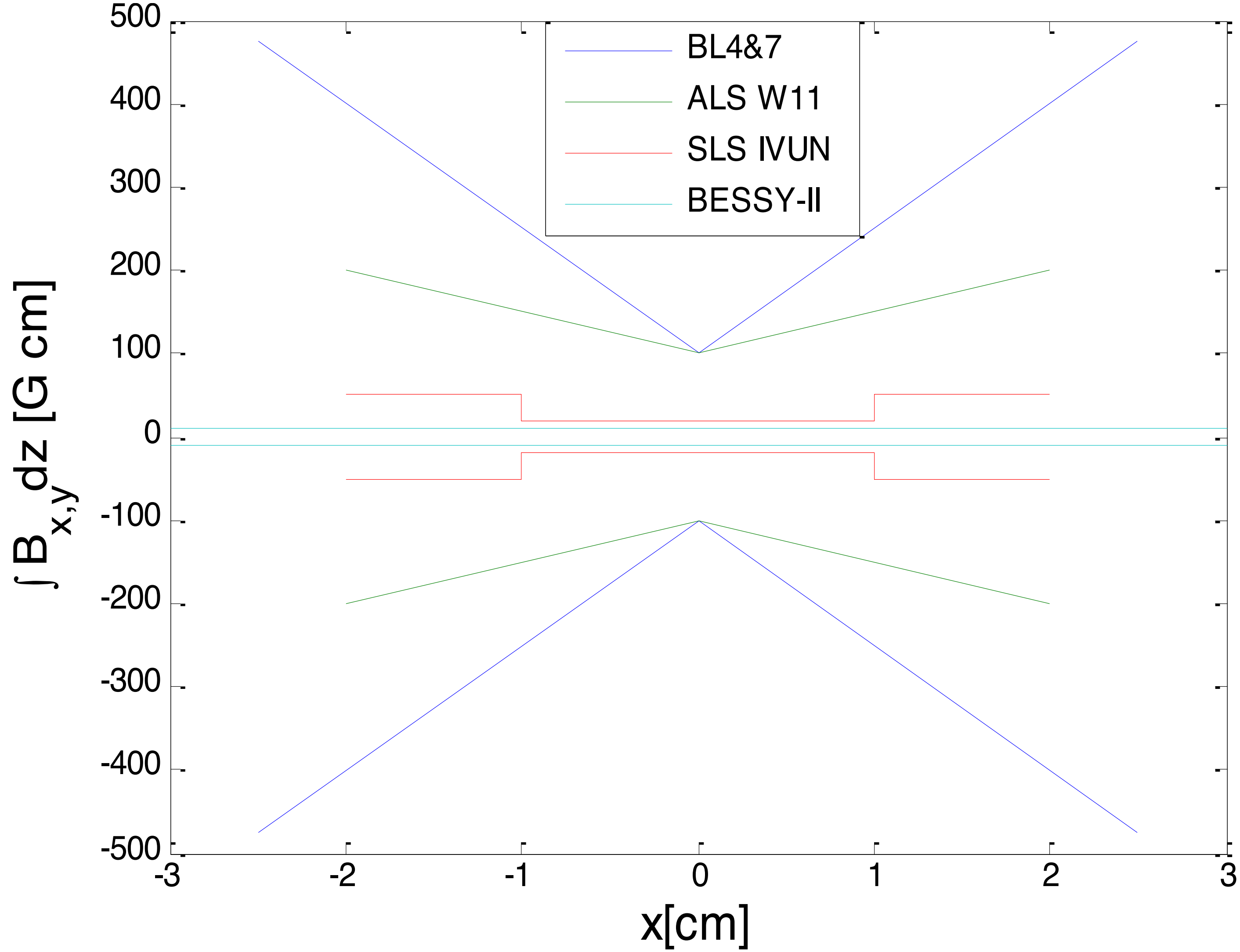

For SSRL BL12 & 13: 100 + 50*|x| G*cm, |x|<2.5 cm; (ALS extended to 25 mm)

Beam-based characterization of BL11 normal multipoles

The tune shift with horizontal orbit was also measured in BL11

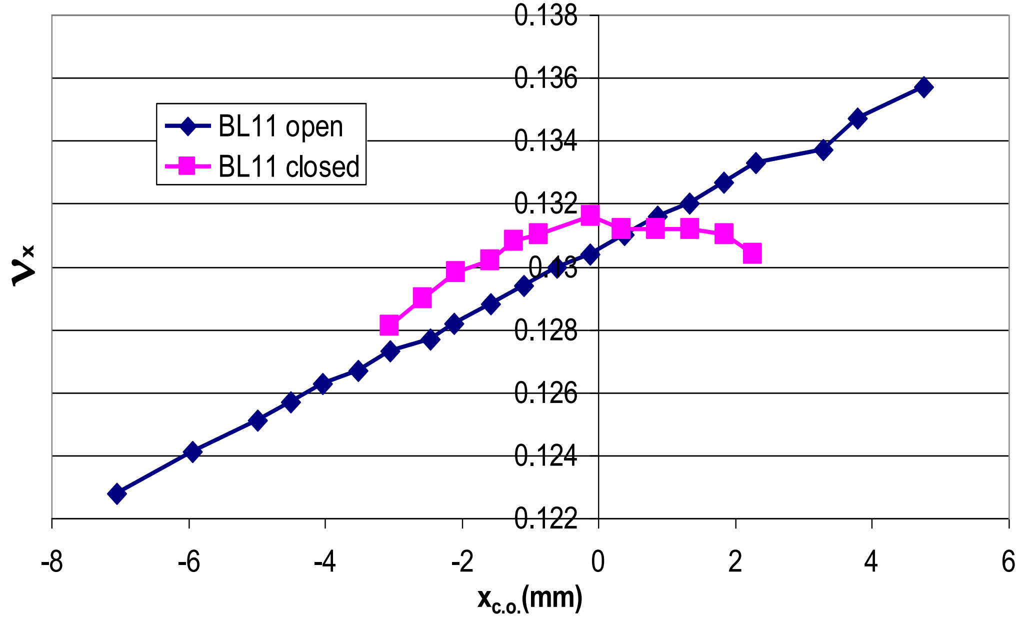

First note that the measurements with BL11 closed extend only a couple millimeters. Due to nonlinear fields, the beam could not be stored with the orbit farther from the center. The large nonlinear fields in BL11 provided impetus for ID beam dynamics measurements at SSRL. When the device was installed in the ring at SSRL, we could no longer hold beam at the 2.3 GeV injection energy with the wiggler gap closed. At 3 GeV, the wiggler decreased the lifetime by 30% due to decrease in the dynamic aperture.

Beam-based characterization of BL11 normal multipoles

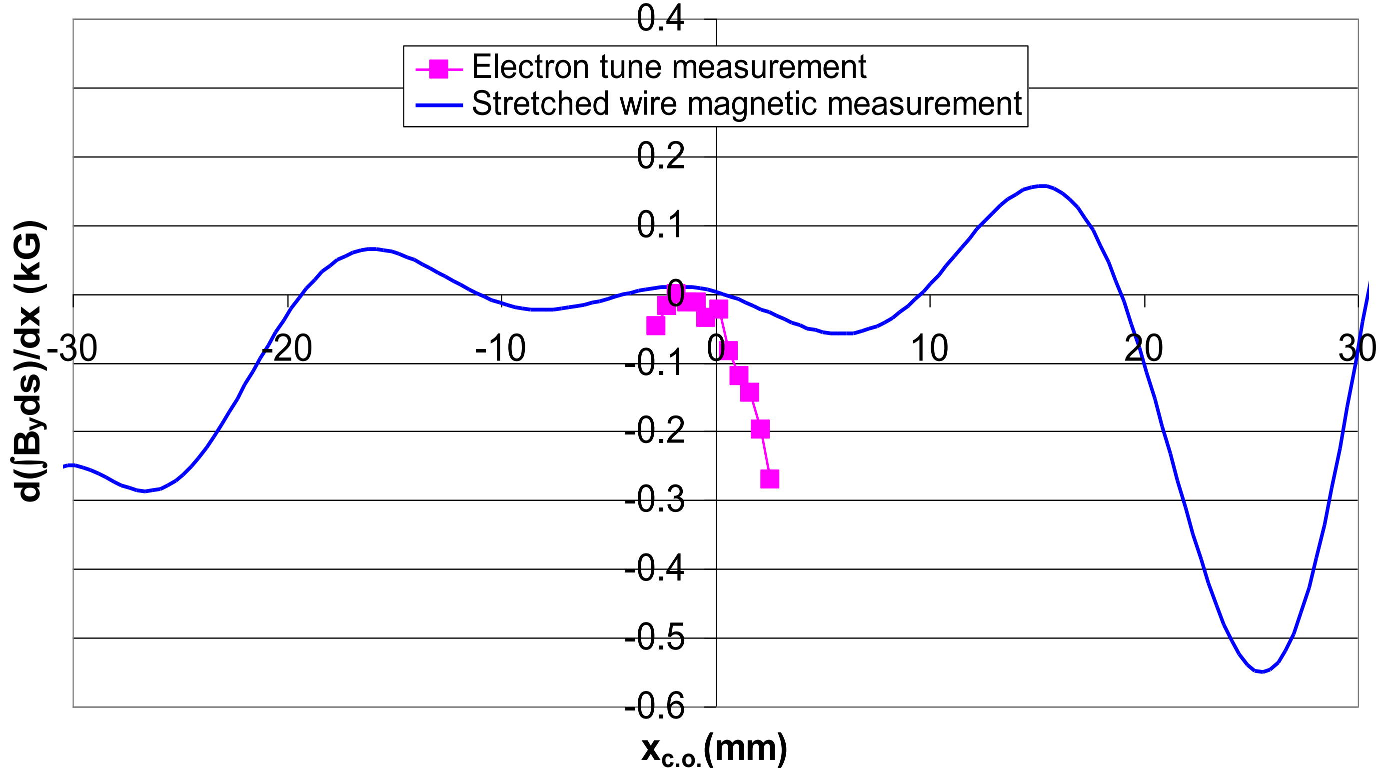

Instead of the nice agreement seen with BL9 wiggler measurements, tune measurements with BL11 indicate nonlinear fields seen by the electron beam that are not seen in magnetic measurements. The quadratic dependence of the tune with the closed orbit indicated a cubic term in the horizontal equation of motion.

The nonlinear fields in BL11 were also characterized by kicking the beam (with an injection kicker) and digitizing the resulting betatron oscillations. NAFF was used to extract the tune vs. amplitude.

- Change in ν_x vs. x_β^2 implies strong x^3 in equation of motion
- Consistent with closed orbit bump measurement.
- Reduced maximum amplitude (BL11 closed) … reduced dynamic aperture.
- N.B. The maximum kick with all other IDs open was 245 mm², so the dynamic aperture had already been reduced by IDs prior to BL11 installation.

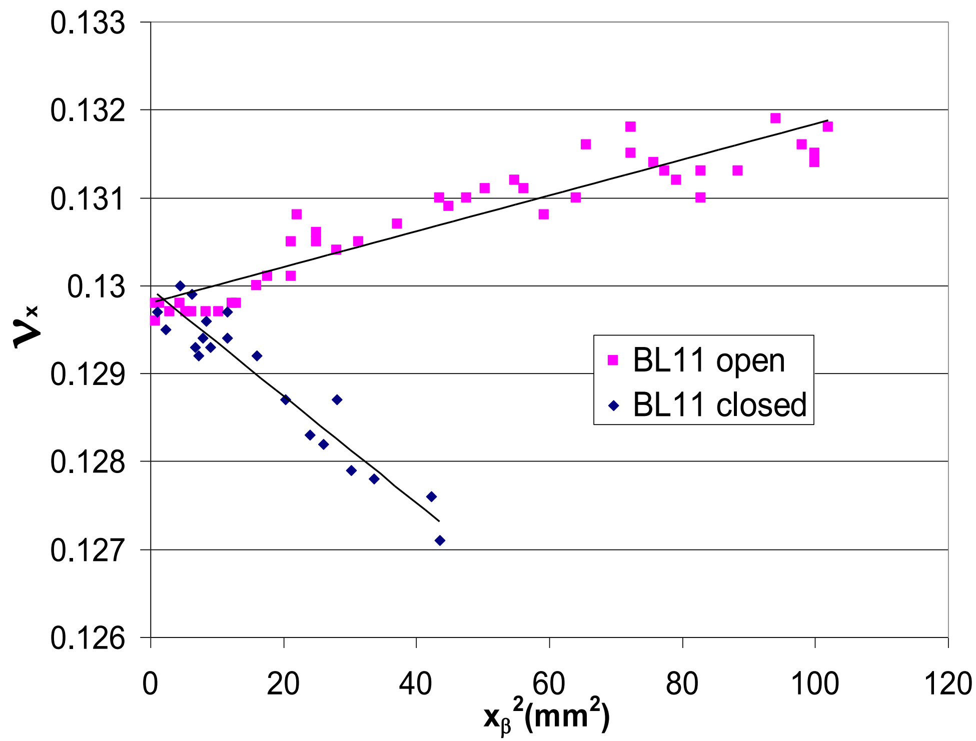

Nonlinear dynamics intrinsic to IDs

Insertion devices (IDs) can have highly nonlinear fields. Nonlinear fields seen by the electron beam come in two flavors: errors from construction tolerances and nonlinear fields intrinsic to the ID design. A linearly polarized ID has a periodic vertical field.

$$B_y(x,y,z) = \sum_{n=1,3,5\ldots} B_n(x,y)\cos nkz$$

The field integral seen along a straight trajectory (i.e. as measured by a stretched wire or flip coil) is zero,

$$\int_0^{m\lambda} B_y(x,y,z)\,dz = 0$$

The field from one pole cancels that from the next. In a real ID, the cancellation is not perfect, due to variations in pole strengths and placement.

Dynamic field integrals

The field integral along a straight trajectory is zero, because the field from one pole is exactly cancelled by the next pole. Because the electron trajectory differs from one pole to the next by $2\hat{x}$, the field integral is nonzero.

$$\int B_y ds \approx \frac{-L}{2k^2 B\rho} B_y(x_i) \frac{dB_y(x_i)}{dx}$$

Dynamic field integral scales as ID period squared and as the derivative of the transverse field roll-off.

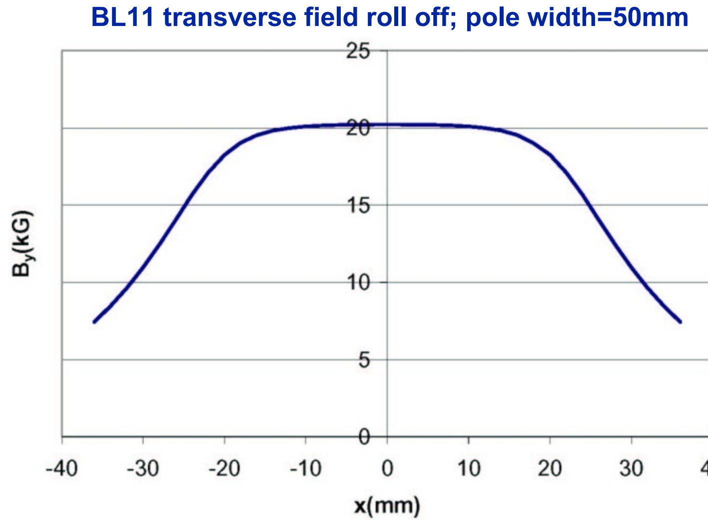

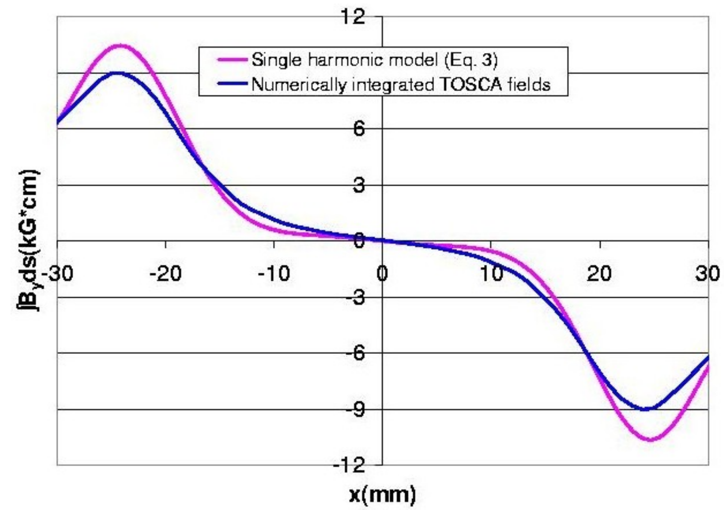

Nonlinear fields intrinsic to IDs: dynamic field integrals

The nonlinear fields in BL11 are only seen along the wiggling electron trajectory. To illustrate this, look at the beam dynamics in the horizontal plane only. For y=0, let $B_y(x,z) = B_y(x)\cos(kz)$

The beam trajectory, x_w, is given by $\dfrac{\partial^2 x_w}{\partial x^2} = \dfrac{B_y(x,z)}{B\rho}$

So for an electron entering the wiggler displaced by x_i

$$x_w = x_i - \hat{x}\cos(kz), \qquad \hat{x} = \frac{B_y(x_w)}{k^2 B\rho}$$ (=155μm for BL11)

The integrated field seen along wiggling trajectory

$$\int B_y ds \approx \int B_y(x_i - \hat{x}\cos(kz))\cos(kz)dz$$

$$= \frac{-L}{2}\hat{x}\frac{dB_y}{dx}$$

So the integrated field seen by the electron as a function of x scales as the derivative of the transverse field roll-off sampled by the wiggling trajectory.

Tune shift from dynamic field integrals

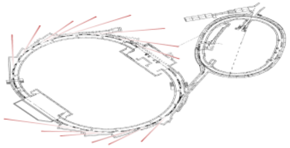

The measurements of tune shift with horizontal closed orbit bump accurately predict the dynamic field integral.

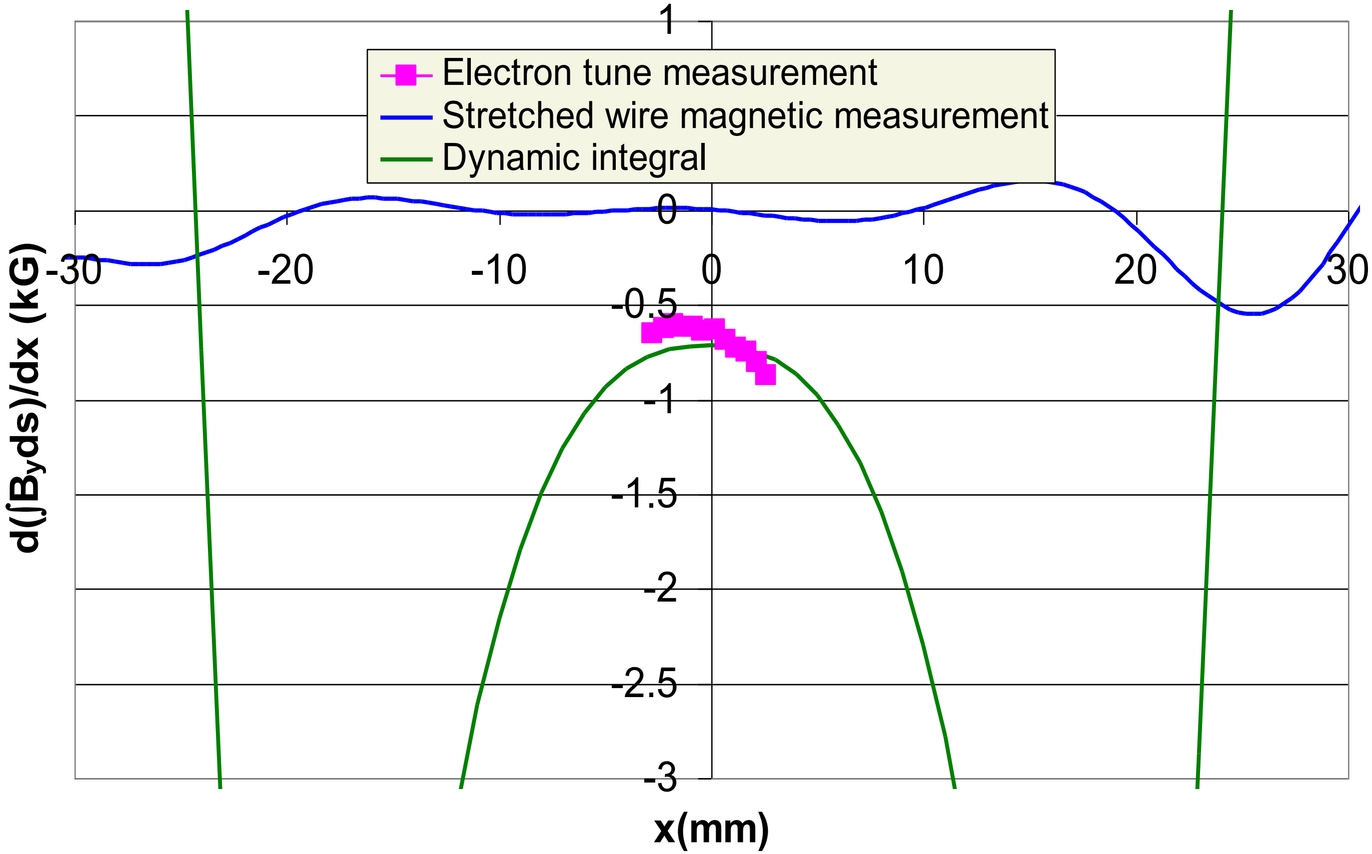

Dynamic aperture with BL11 nonlinear fields

A computer code model of BL11 (with BETA) showed that the strong nonlinear fields severely distort the dispersion and limit the off-energy dynamic aperture.

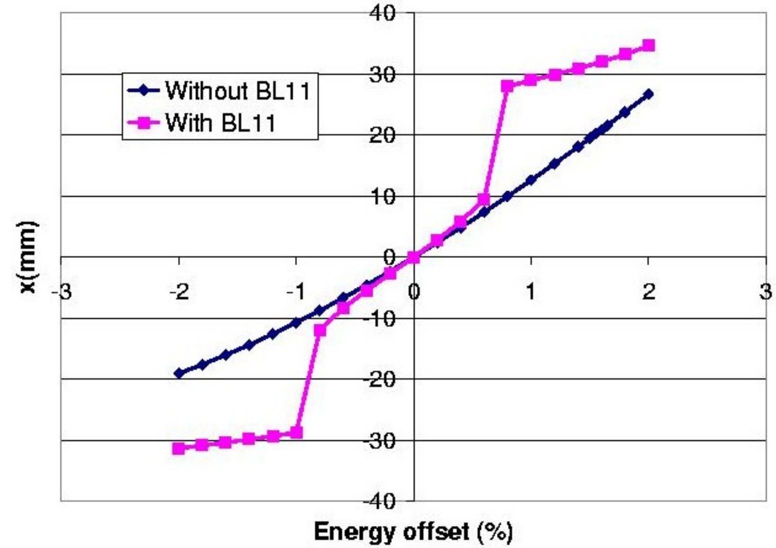

This explains the reduction in lifetime and troubles with injection.

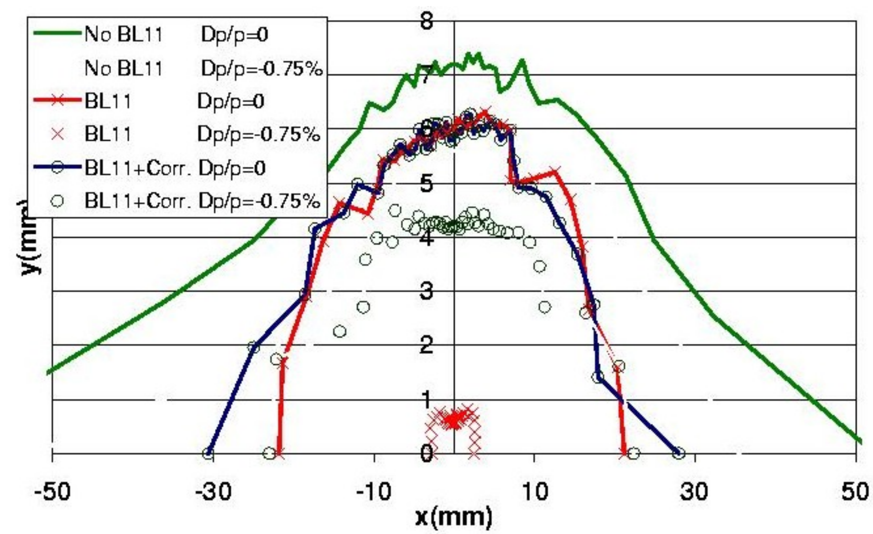

Magic finger correctors for BL11

Nonlinear corrector magnets (magic fingers) were installed at each end of the wiggler to cancel the dynamic integrals.

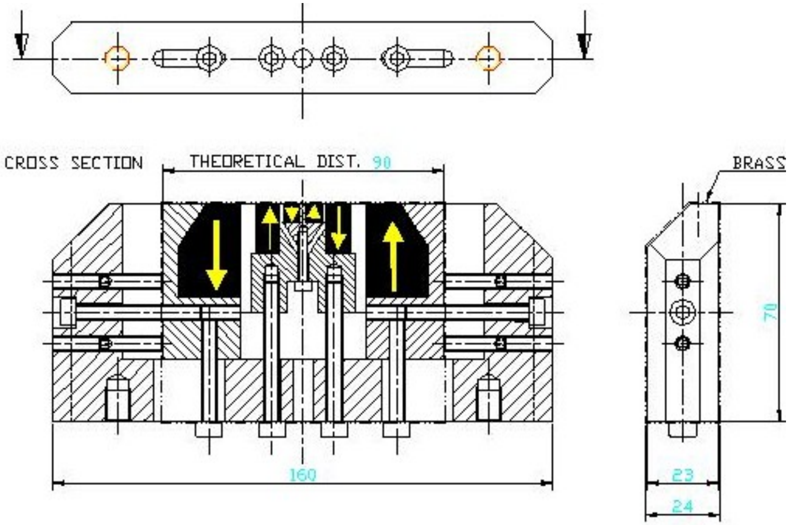

The bottom half of the magic fingers for one end of the wiggler. The yellow arrows indicate polarity of permanent magnets. The magnet is ~1” long.

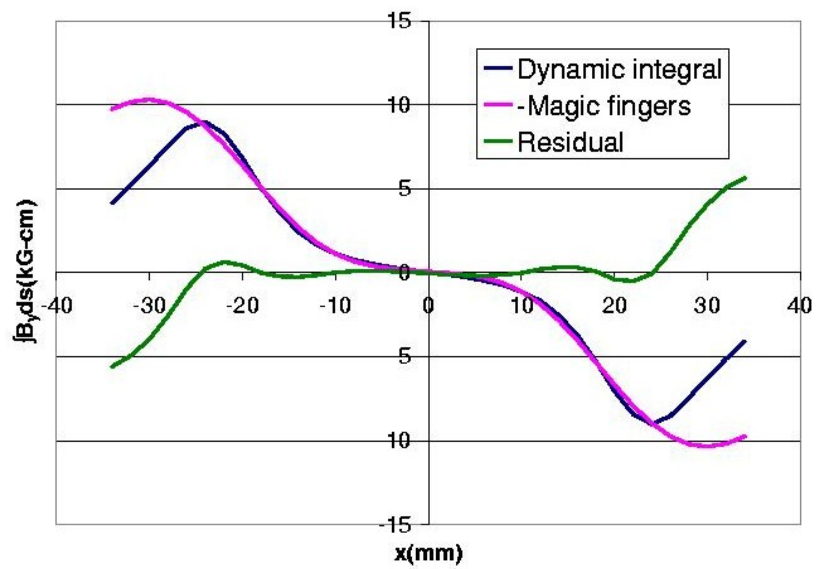

Field integral correction achieved with magic fingers.

Improvement from magic fingers

Without magic fingers:

With magic fingers:

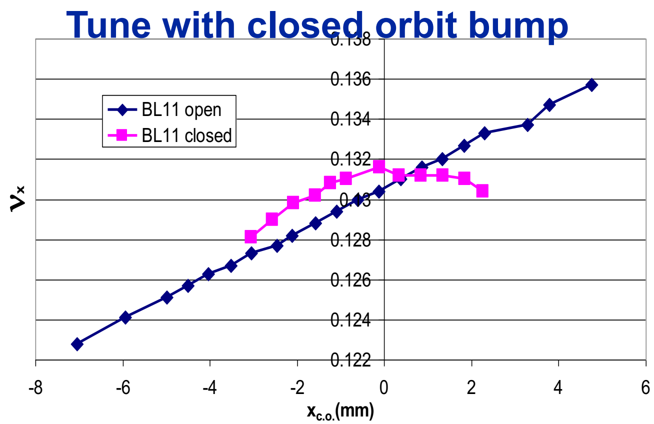

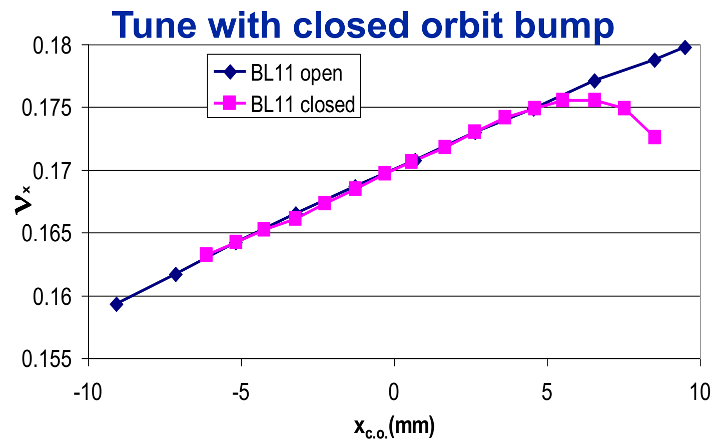

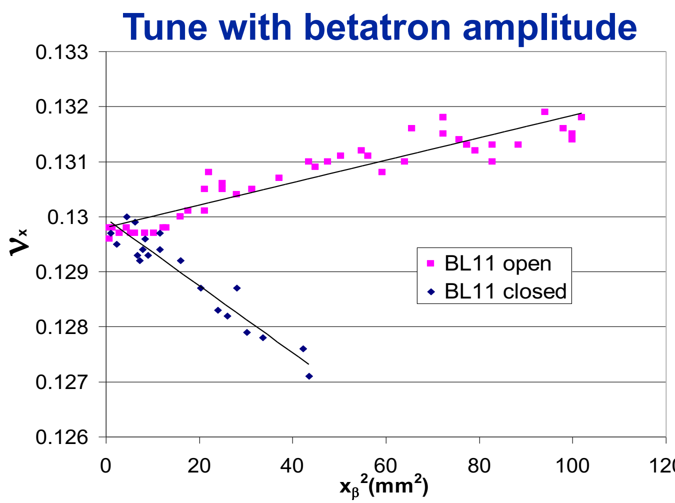

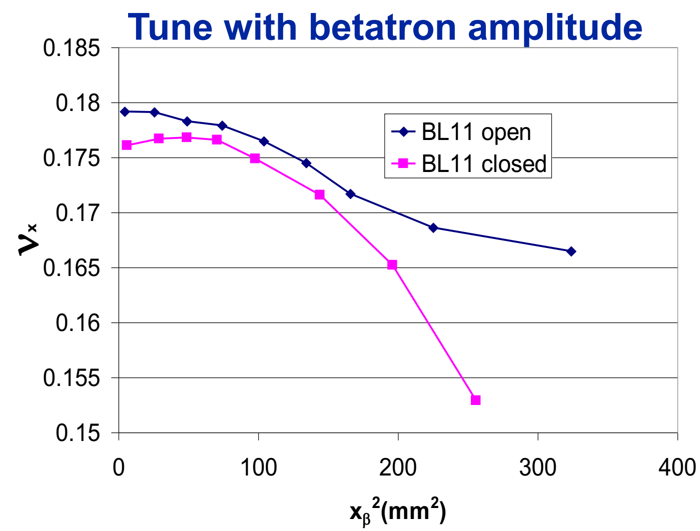

Magic finger correction imperfect

Figure shows the magnitude of the field integral from BL11 as a function of (x,y). The magnitude of the kick received by the beam passing through the wiggler is

$$|\vec{\theta}| = \frac{1}{B\rho} \left| \int (B_x, B_y) ds \right|$$

Without magic fingers:

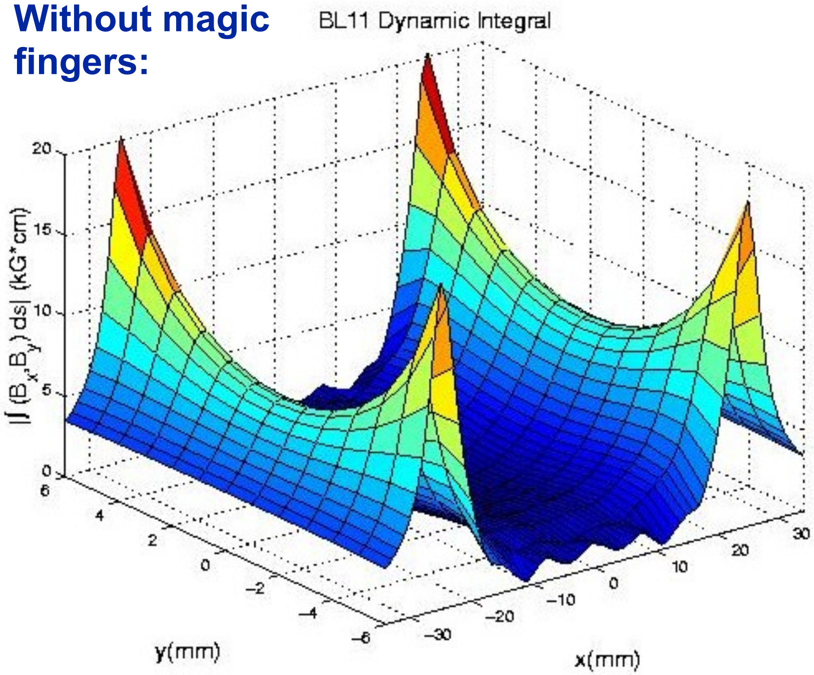

Magic fingers are thin lens multipoles, so field integrals are given by

$$\int (B_x + iB_y) ds = -B\rho \sum_n (b_n + ia_n)(x+iy)^{n-1}$$

The dynamic integrals do not have this form, so the magic fingers are not effective over all (x,y).

With magic fingers:

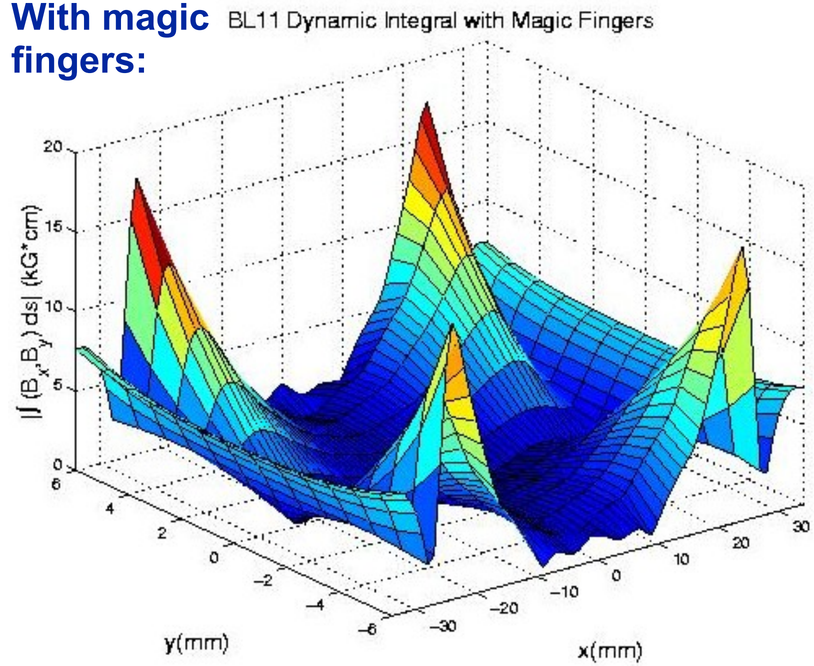

SSRL ID field integral specifications

- On-axis (x=y=0) specifications, normal, b_n, and skew, a_n
  - Integrated quadrupole < 50 G
  - Integrated sextupole < 75 G/cm
  - Integrated octupole < 40 G/cm^2

$$\int (B_x - iB_y)dz = \sum (a_n + ib_n)(x+iy)^n$$

- Off-axis specifications
  - 1st integral of B_y < 100 + 50*|x| G*cm, |x|<2.5 cm
  - 1st integral of B_x < 40 + 75*|x| G*cm, |x|<2.5 cm
  - 2nd integral of B_y < 1.5e4+1e4*|x| G*cm^2, |x|<2.5 cm.
  - 2nd integral of B_x < 5e3+1e4*|x| G*cm^2, |x|<2.5 cm
  - 1st integral deriv. < 50+150*|x| G; |x|<2.5 cm, $\frac{\partial}{\partial x}\int B_{x,y}dz$
- Peak field transverse roll-off
  - dB_y/dx < 11000+5500*|x| G/cm, |x|<2.5 cm (BL12)
  - dB_y/dx < 870+440*|x| G/cm, |x|<2.5 cm (BL13)
  - d^2B_y/dx^2 < 15000+20000*|x| G/cm^2, |x|<2.5 cm (BL12)
  - d^2B_y/dx^2 < 1200+1500*|x| G/cm^2, |x|<2.5 cm (BL13)
- Accelerator physics group will review fields, once the ID is designed.
- Accelerator physics group will review magnetic measurements plan.

Controls static (construction tolerance) field integrals

Controls dynamic field integrals (intrinsic to magnet design)

ID field integral scaling

- **with energy**
  - Static integrals scale as $1/E$ { $\theta = BL/B\rho$ = (0.3 GeV/Tm)*BL/E }
  - Dynamic integrals scale as $1/E^2$ (one E from $d\theta$, one E from wiggle amplitude)
- **with ID period**
  - Dynamic vertical octupole-like term ($y'' \sim y^3$) *scales as* $1/\lambda^2$ (trouble for short period IDs)
  - Dynamic integrals associated with transverse field roll-off scale as λ^2 (trouble for long period IDs)

CESR superconducting wiggler

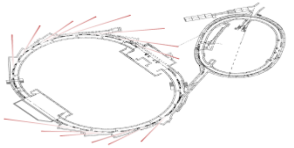

1. **Tune vs. closed orbit measurements confirmed expected field integrals.**
2. **Vertical beam size as a function of (ν_x, ν_y) shows resonances excited by wiggler.**

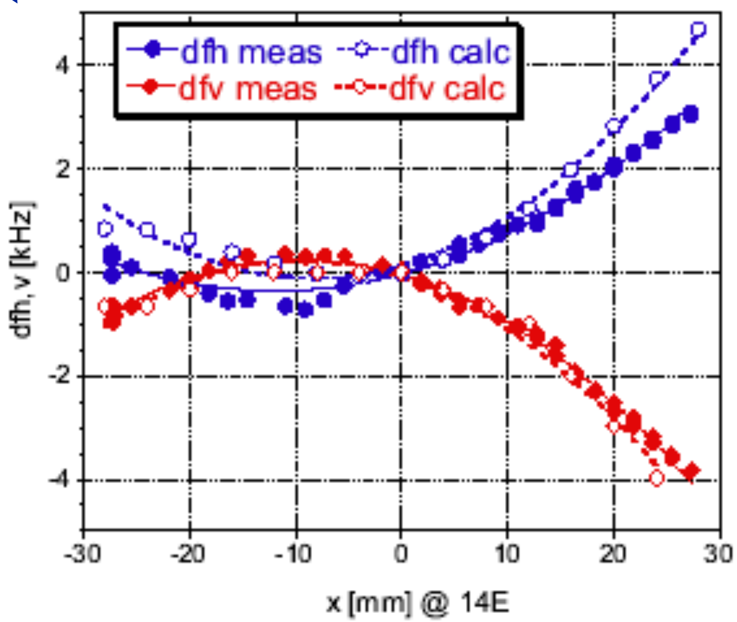

Temnykh et al., PAC03

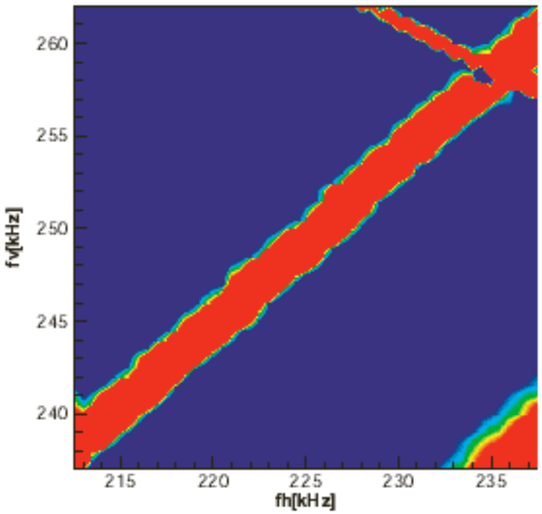

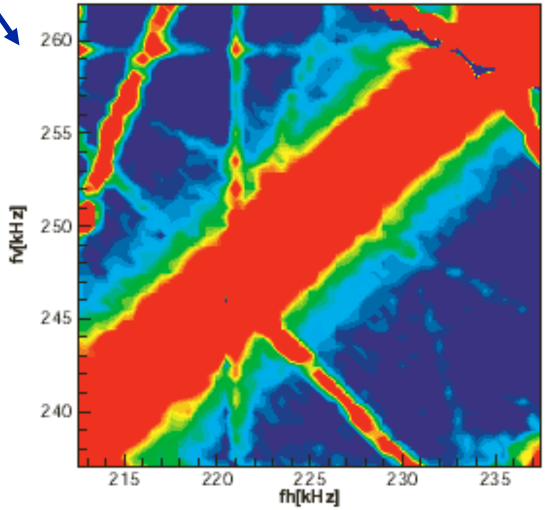

Transverse field roll-off in 4-row EPUs

- Fast roll off in B_x vs. x is unavoidable.
  - With planar IDs, wide magnet poles eliminate B_y vs. x roll-off
  - In EPUs B_x vs. x roll-off is independent of pole width

Max-lab EPU transverse field roll-off →

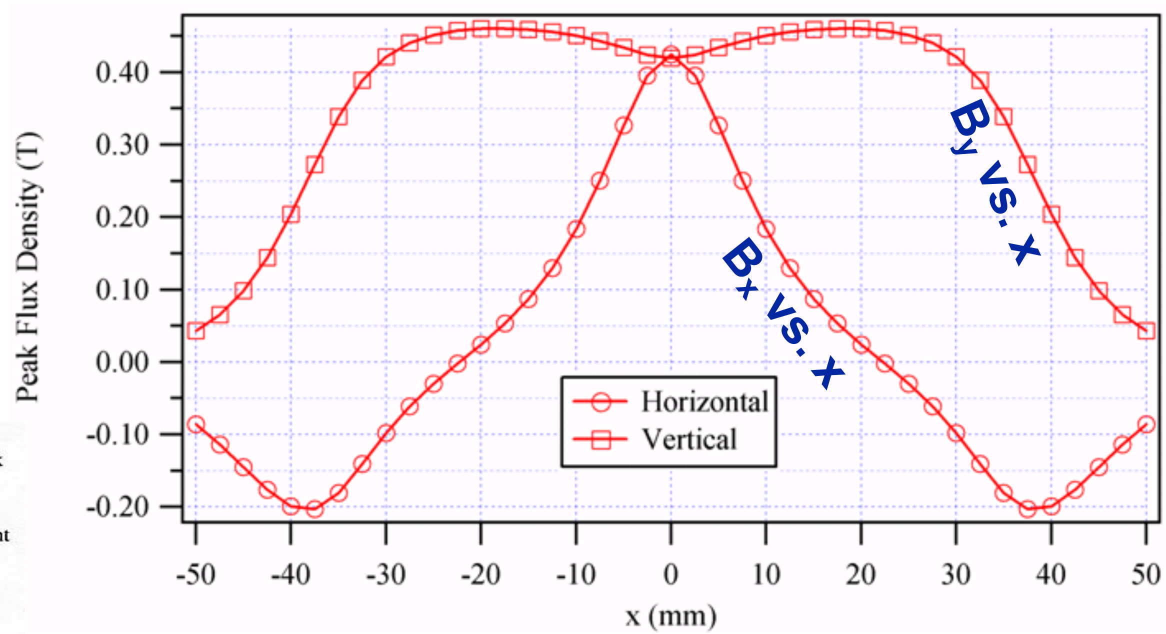

Figure 24. The transverse roll off for the Circular undulator phase.

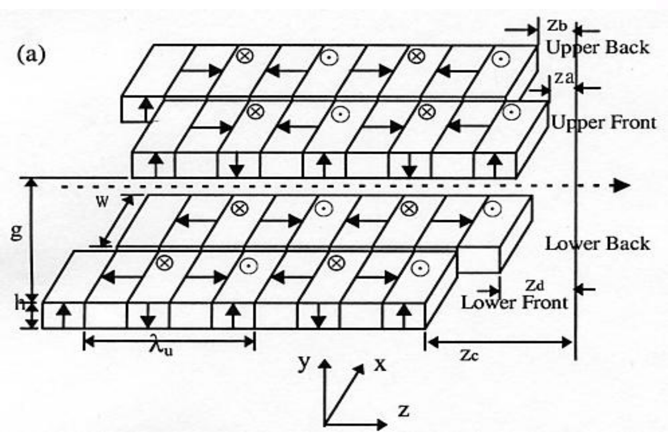

EPU field roll-off with y

- **Fields in EPUs roll off quickly with y as well as x.**
- **Wiggling/spiraling motion takes derivatives of these field roll-offs as well, adding to dynamic integrals.**

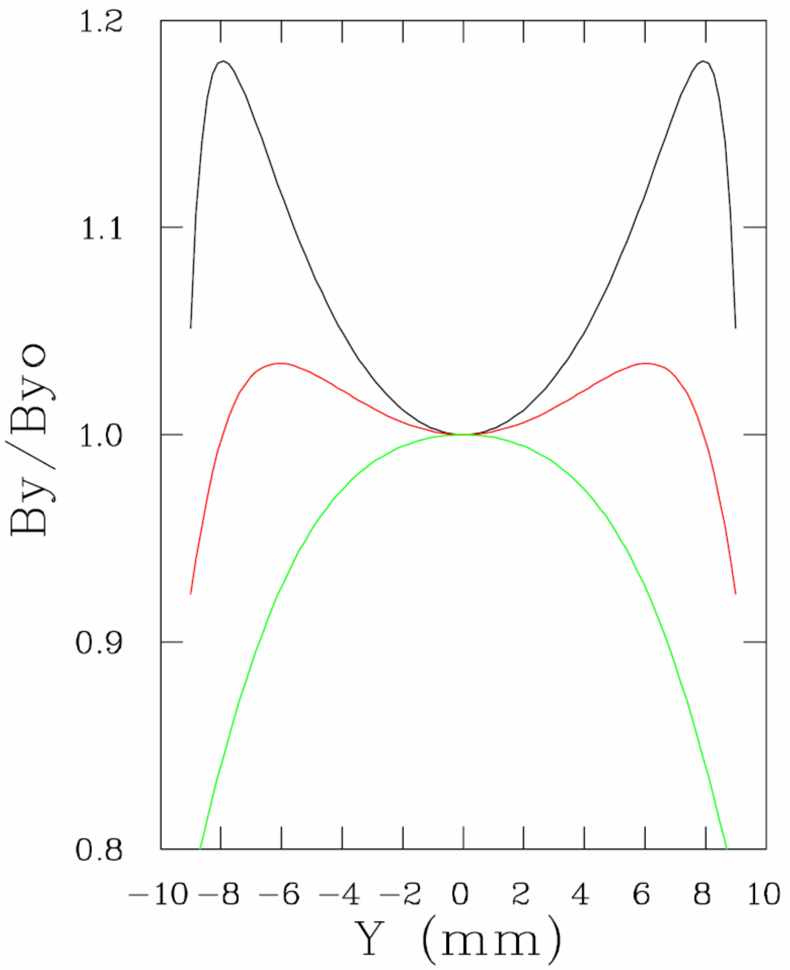

Transverse roll-off of the magnetic field for three different polarization settings of an ALS EPU (C.Steier).

Dynamic integrals in EPUs

I. Blomqvist

- Spiraling trajectory couples with field roll-off, generating field integrals.
- Field integrals vary with row phase and ID gap, so fixed-field nonlinear correctors would not help.

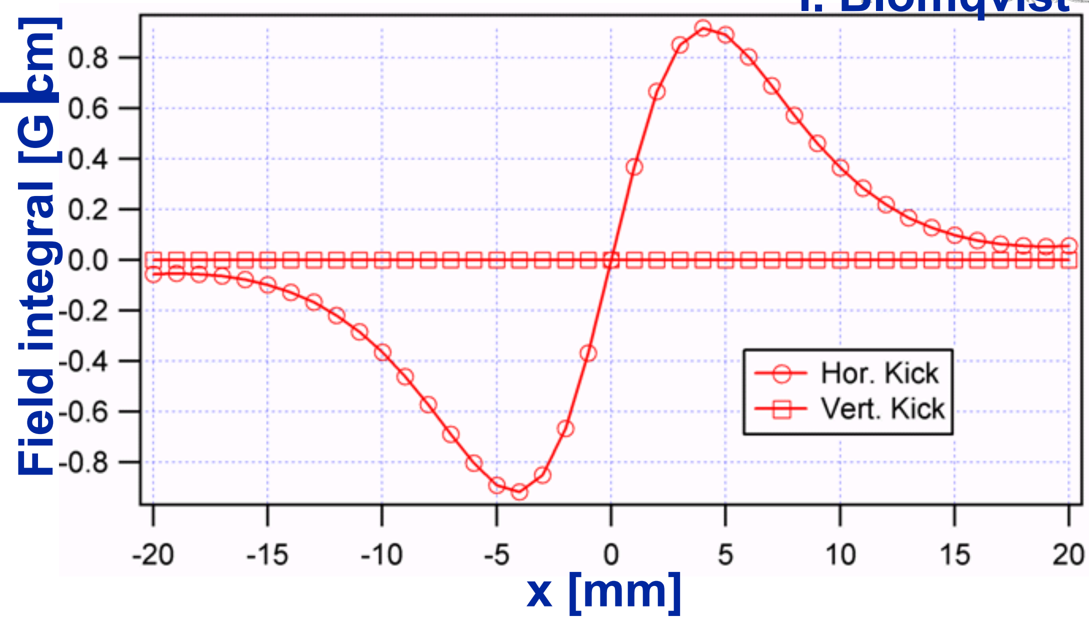

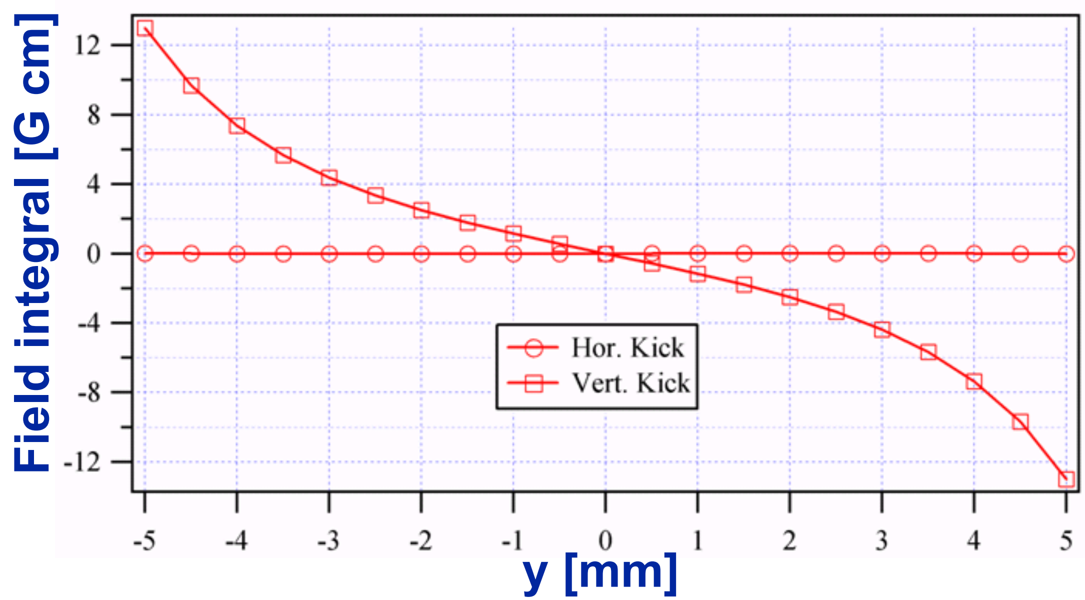

Bessy II measurements with EPUs (before shims)

Tune scans with beam loss monitor measurements can be used to identify resonances excited by IDs.

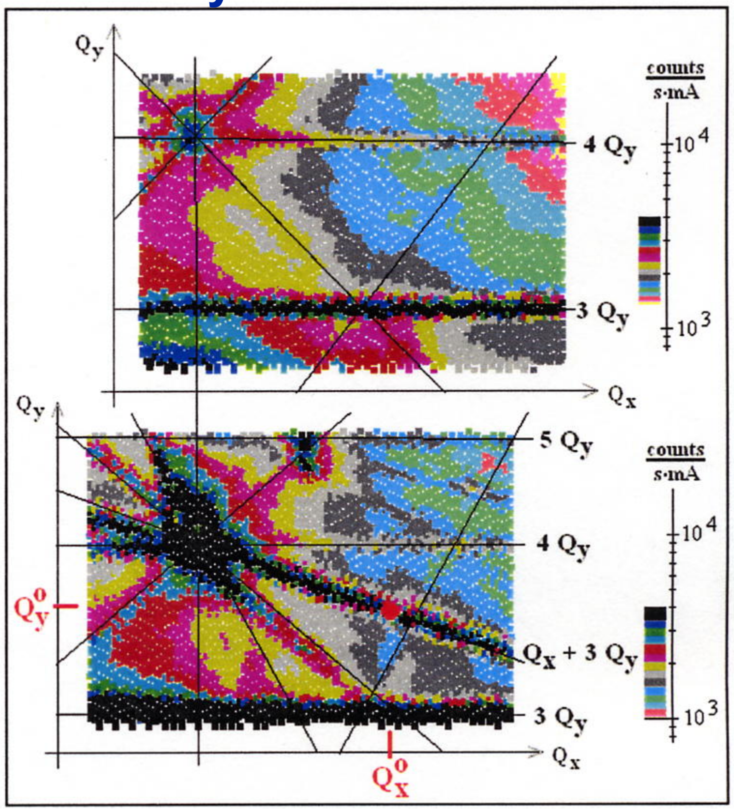

Kuske, Gorgen, Kuszynski, PAC'01

Scanning both tune and closed orbit while measuring lifetime gives a measure of multipole strengths vs. orbit.

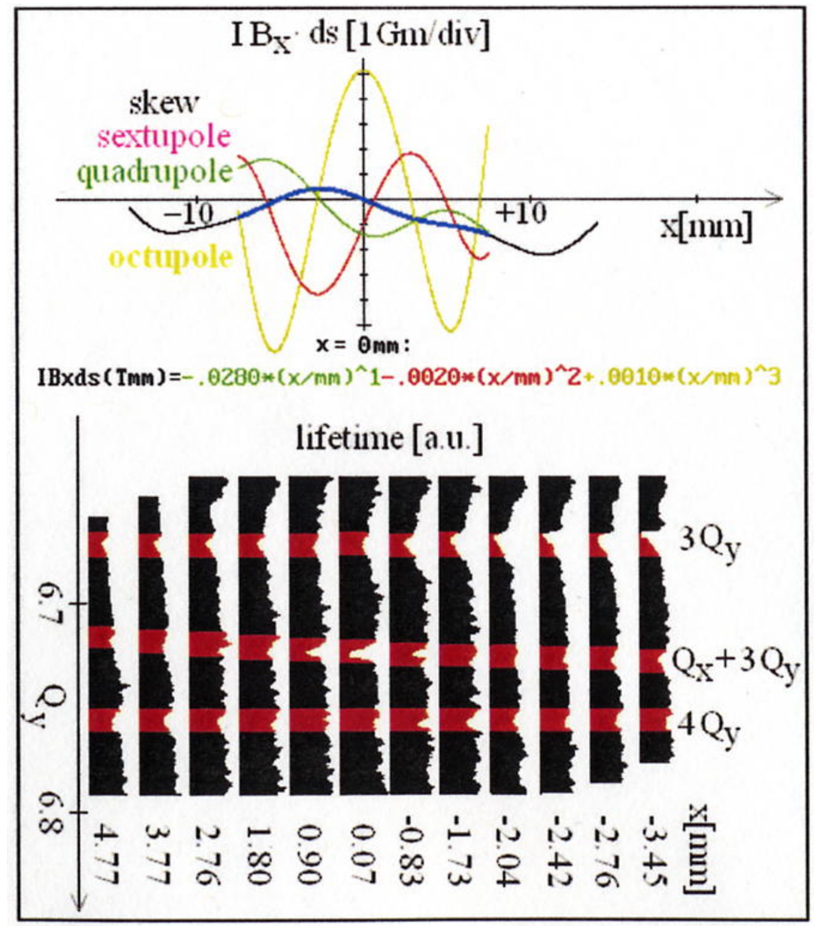

More BESSY II measurements

- Resonance excitation seen in turn-by-turn BPM data.

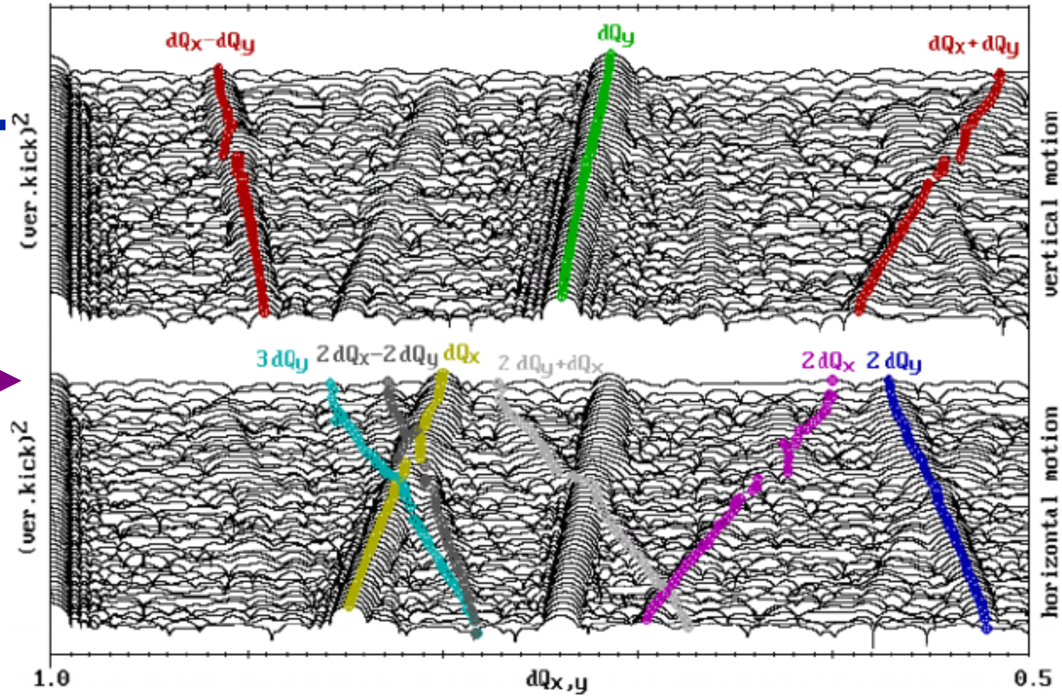

Figure 1: Spectra of the vertical and horizontal beam motion (top and bottom) with the fundamental tunes: dQ_x (yellow), dQ_y (green) and combinations of them.

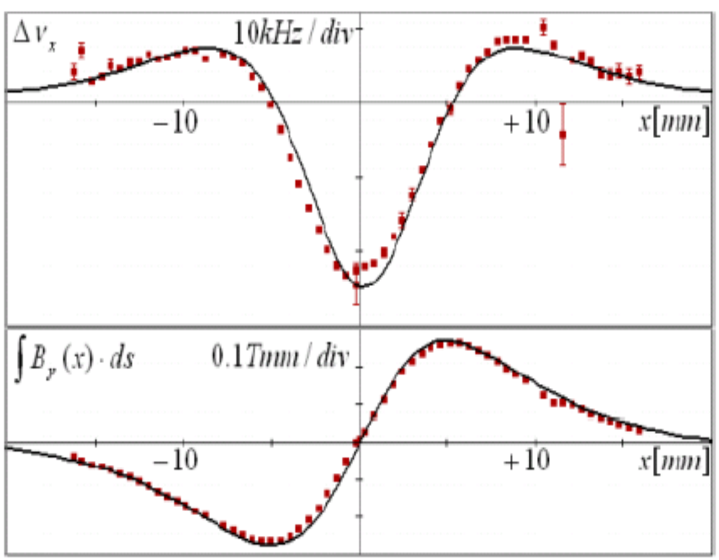

Tune measurements vs. closed orbit bump confirm expected dynamic field integrals.

Frequency map measurements at BESSY-II

Frequency maps have been used to characterize EPU nonlinearities at BESSY-II.

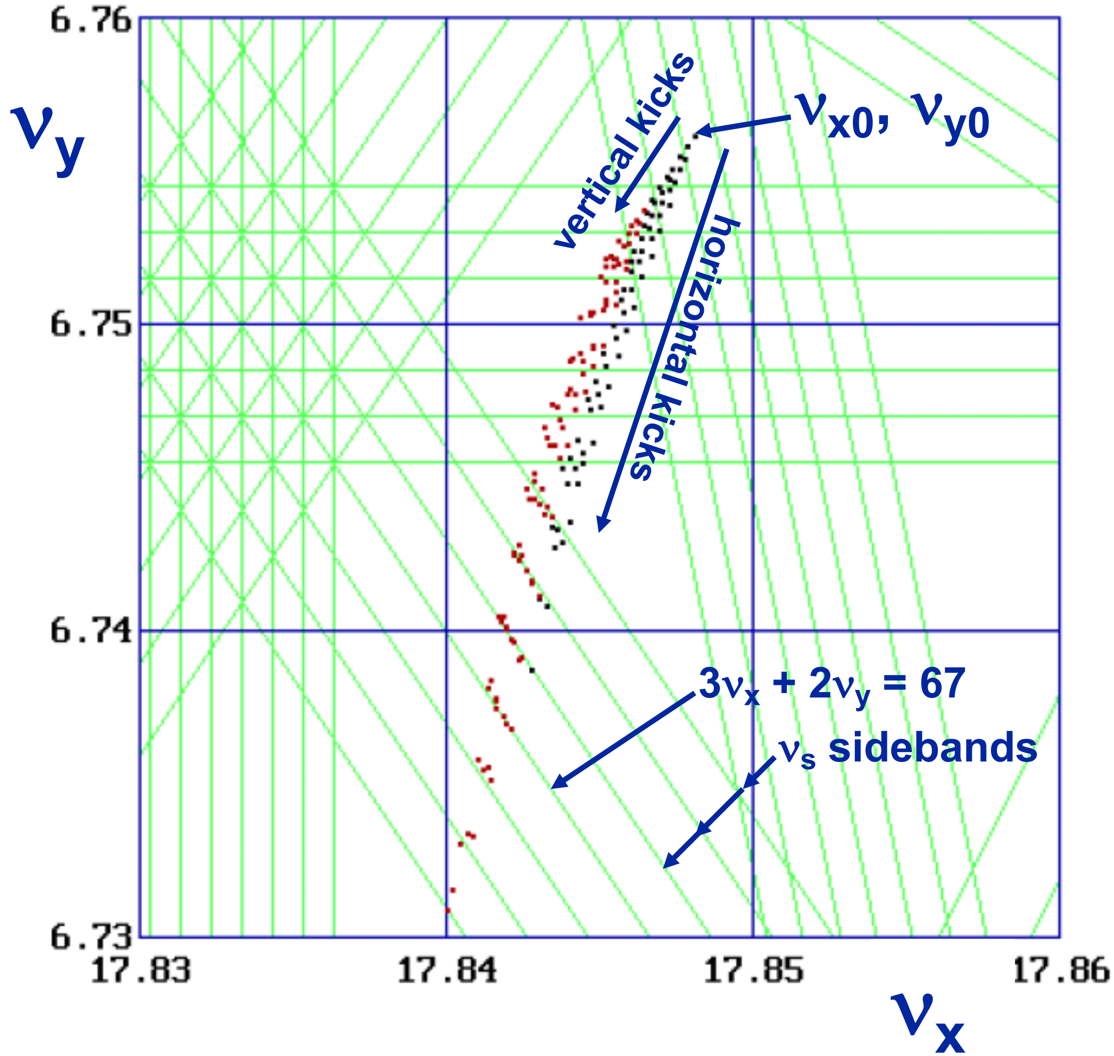

Frequency map measurements at BESSY-II

- Beam dynamics highly dependent on EPU row phase.
- Dynamic aperture reduction induced injection losses

Vertical field

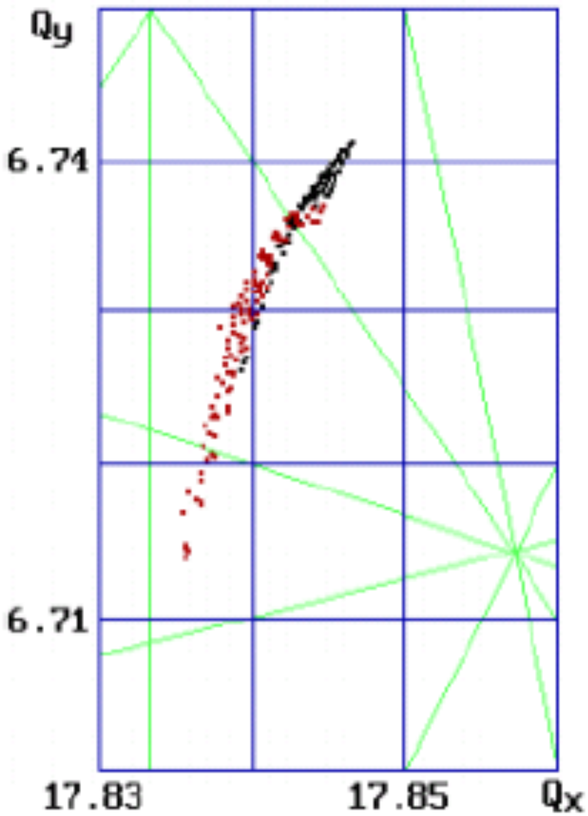

Circular polarization

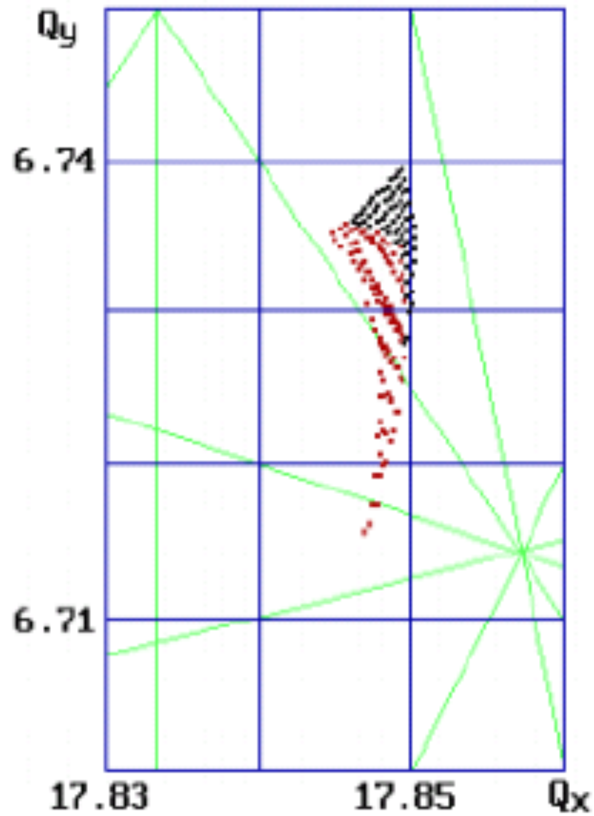

Horizontal field

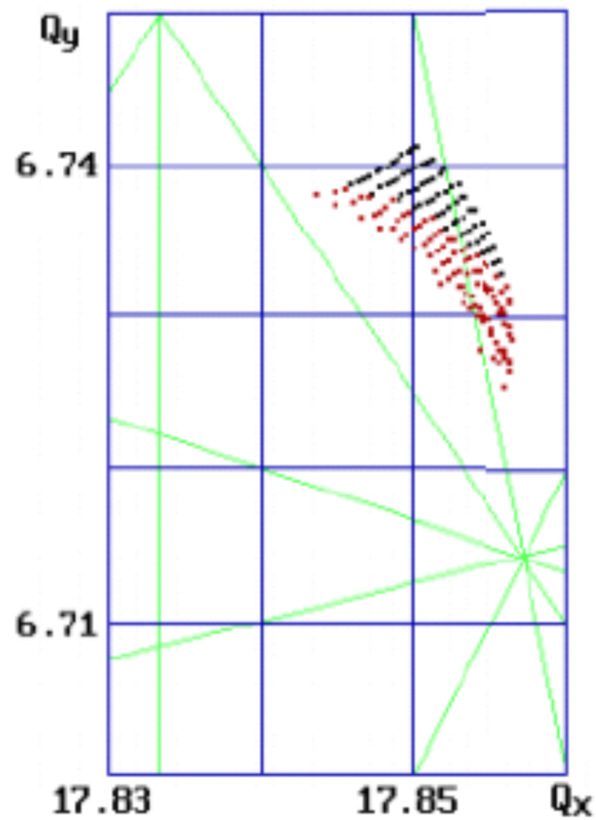

Shims partially correct field integrals

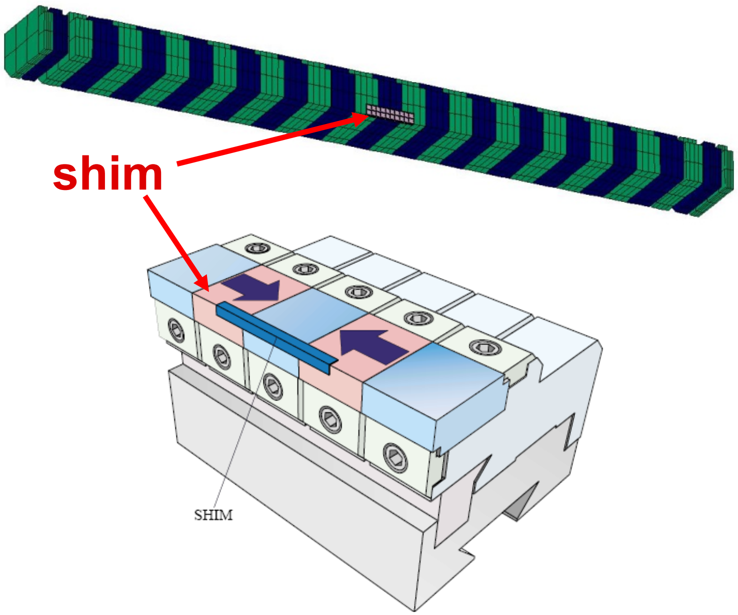

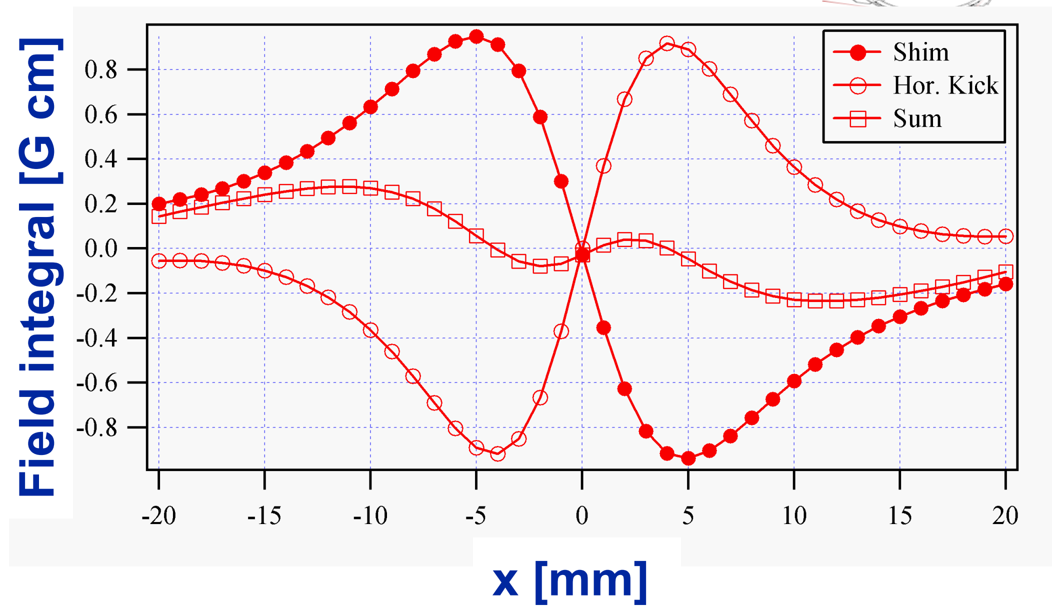

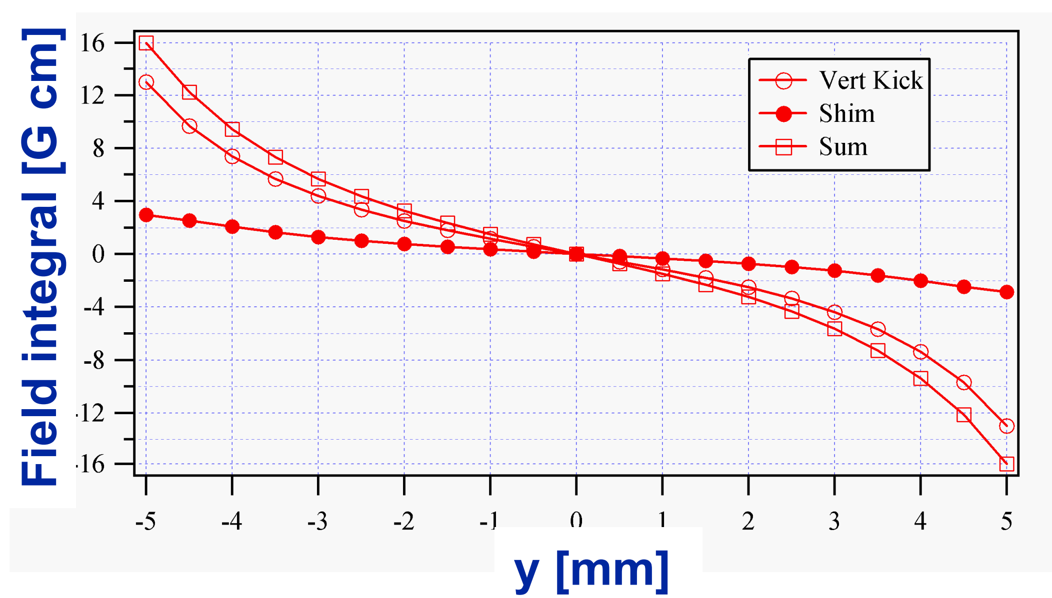

Shims correct field integrals in x-plane, but make integrals a bit worse in y-plane.

Overall beam dynamics improves.

BESSY II frequency maps with shims

- Before shims: Horizontal dynamic aperture and injection efficiency improved with shims.
- After shims: Vertical dynamic aperture decreased

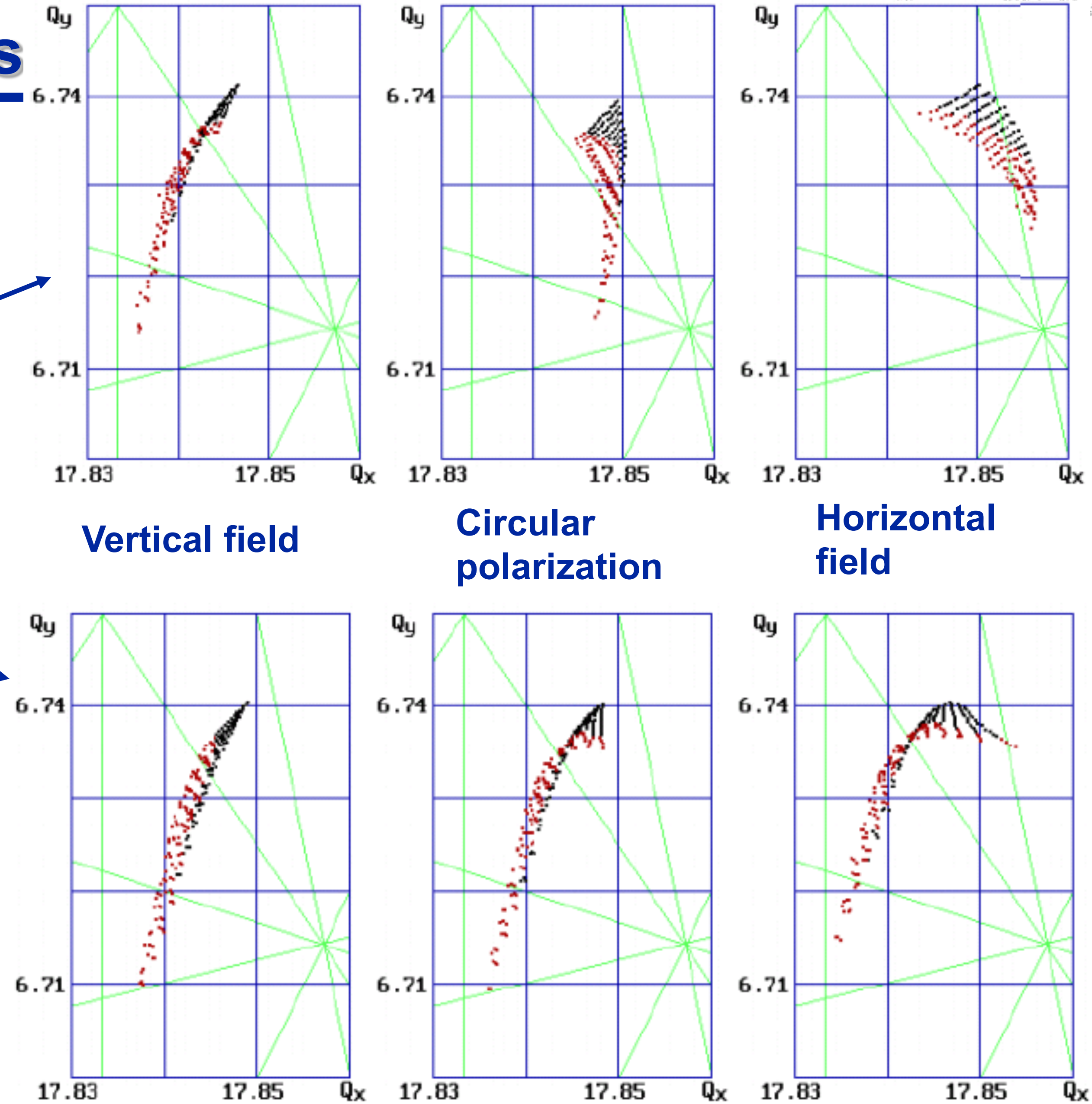

Correction via passive shims

- Dynamic multipoles compensated by magnetic shims

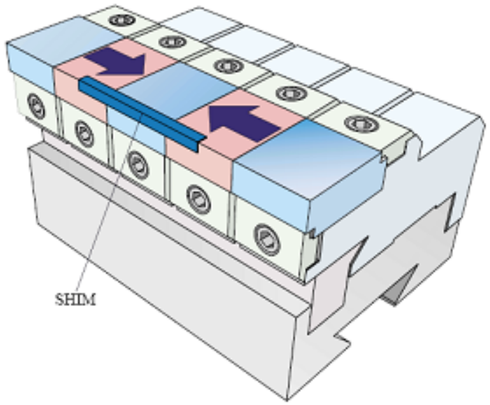

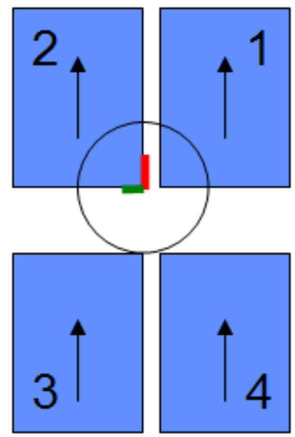

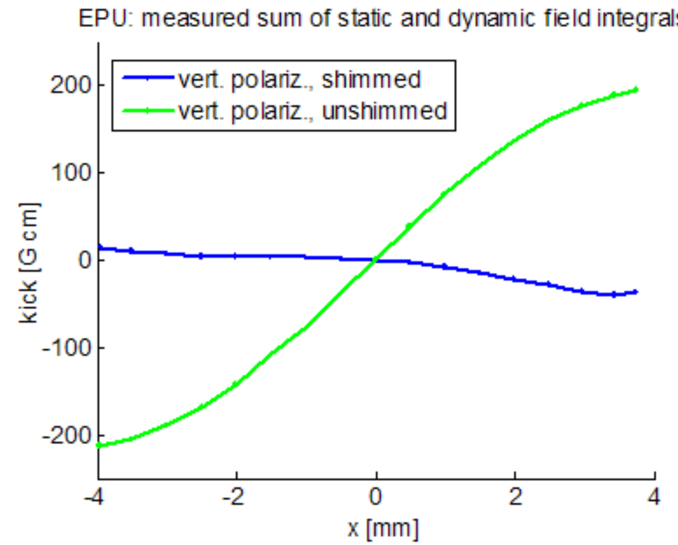

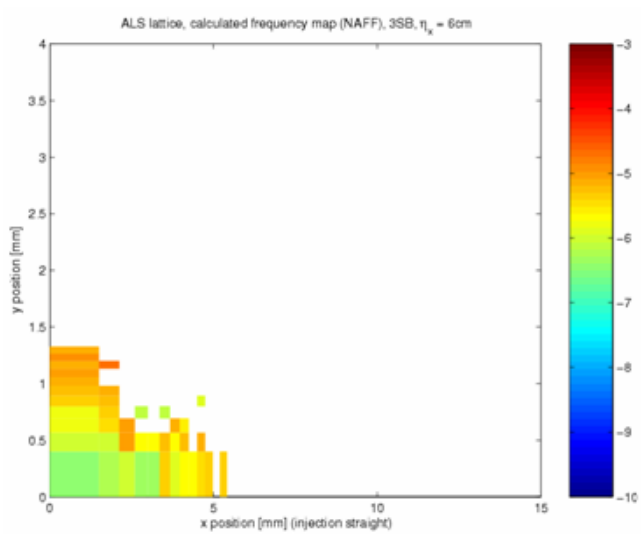

Shimming

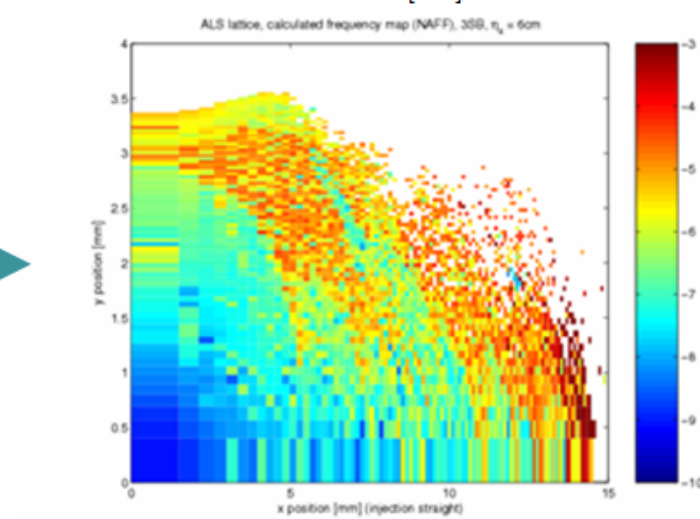

Characterizing shim performance, ALS

- Shims correct nonlinearities for ALS Merlin long-period EPU.
- Shims are ineffective for 45 degree linear mode (shown in black)

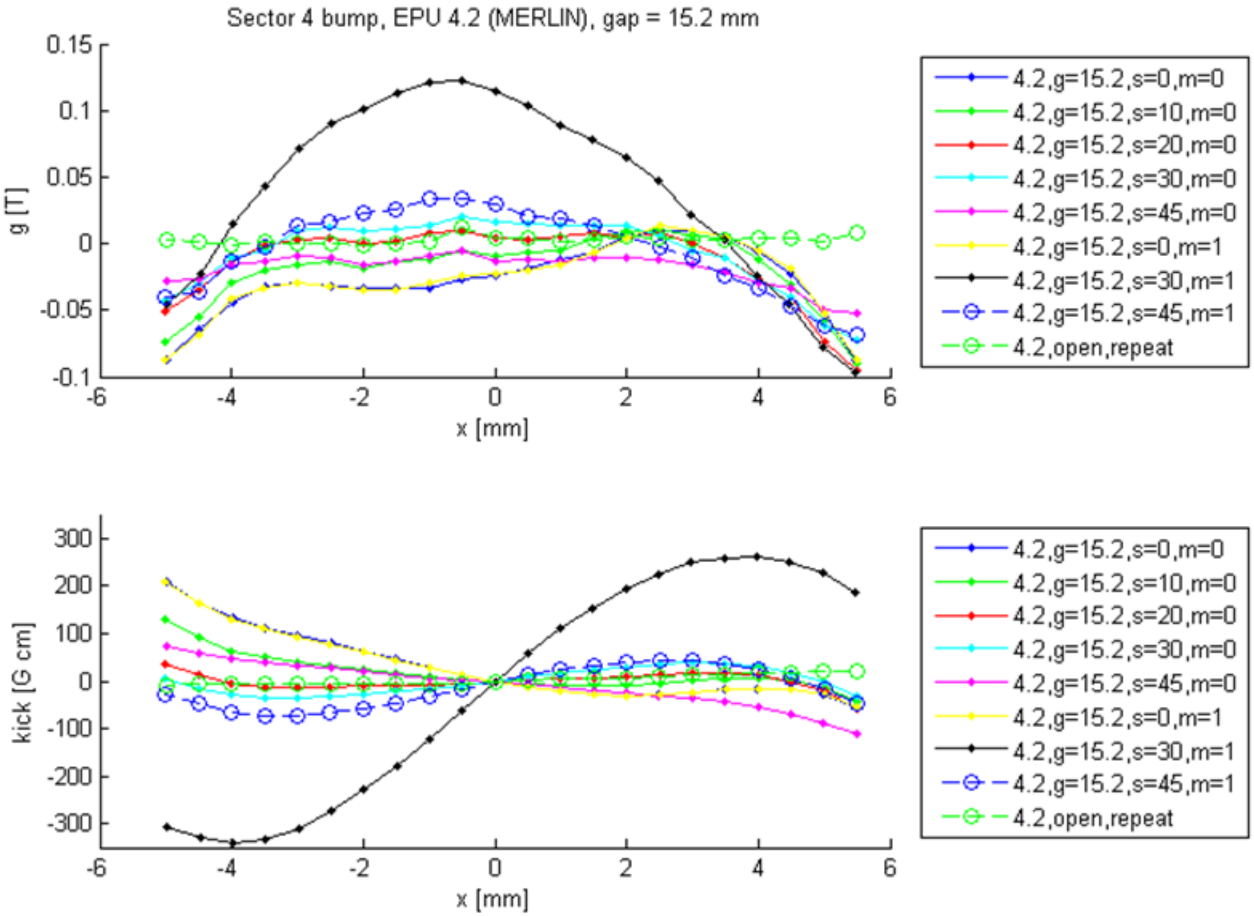

C. Steier

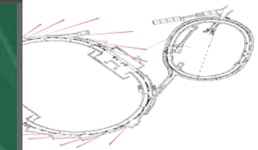

BESSY

UE112ID7R

active compensation of dynamic field componentsin the linear/inclined mode

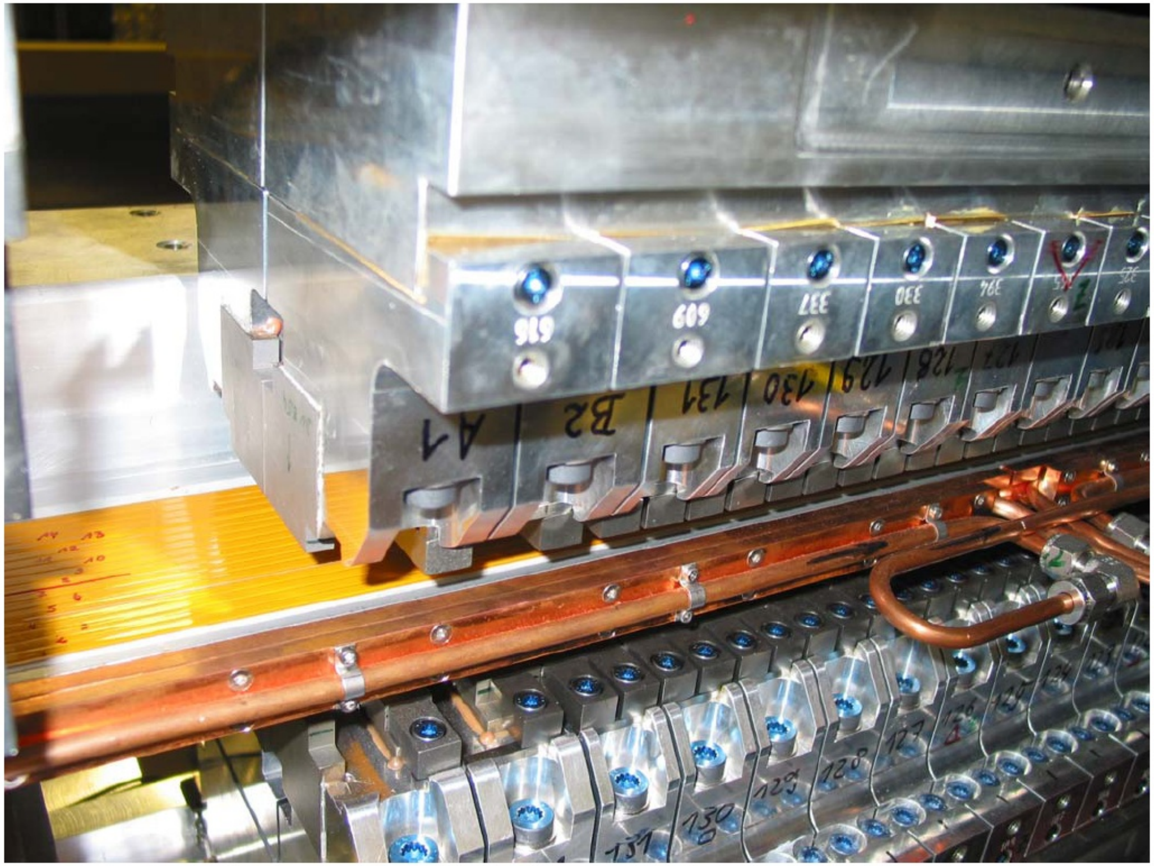

32 flat wires along the ID-chamber with 16 individual PS

P. Kuske, Non-Linear Beam Dynamics Workshop, ESRF, 28th May 2008

http://www.esrf.eu/Accelerators/Conferences/non-linear-beam-dynamics-workshop/

Kuske presentation, 28 May, 2008

Tracking models for EPUs

- For most tracking, we use P. Elleaume type tracking tables from the beta code.
  - Elleaume, Pascal, “A new approach to the electron beam dynamics in undulators and wiggler”, EPAC’92, page 661.
  - RADIA code web reference
- We have also used Ying Wu type symplectic integrators for some tracking studies.
  - Y. Wu, E. Forest, D. Robin, “Explicit Sympectic Integrator for s-dependent Static Magnetic Field”, Phys Rev. E, 2003. (and PAC papers)

Multi-bunch instabilities from SPEAR3 BL15 in-vacuum undulator

K. Tian et al.
SLAC

- Stainless steel cylindrical chamber more than 2 meters long with transitions to standard chambers at both ends.
  - Cut-off frequency of standard chamber ~2 GHz
  - The resonant frequencies of the trapped RF modes in the IVU should be less than 2 GHz

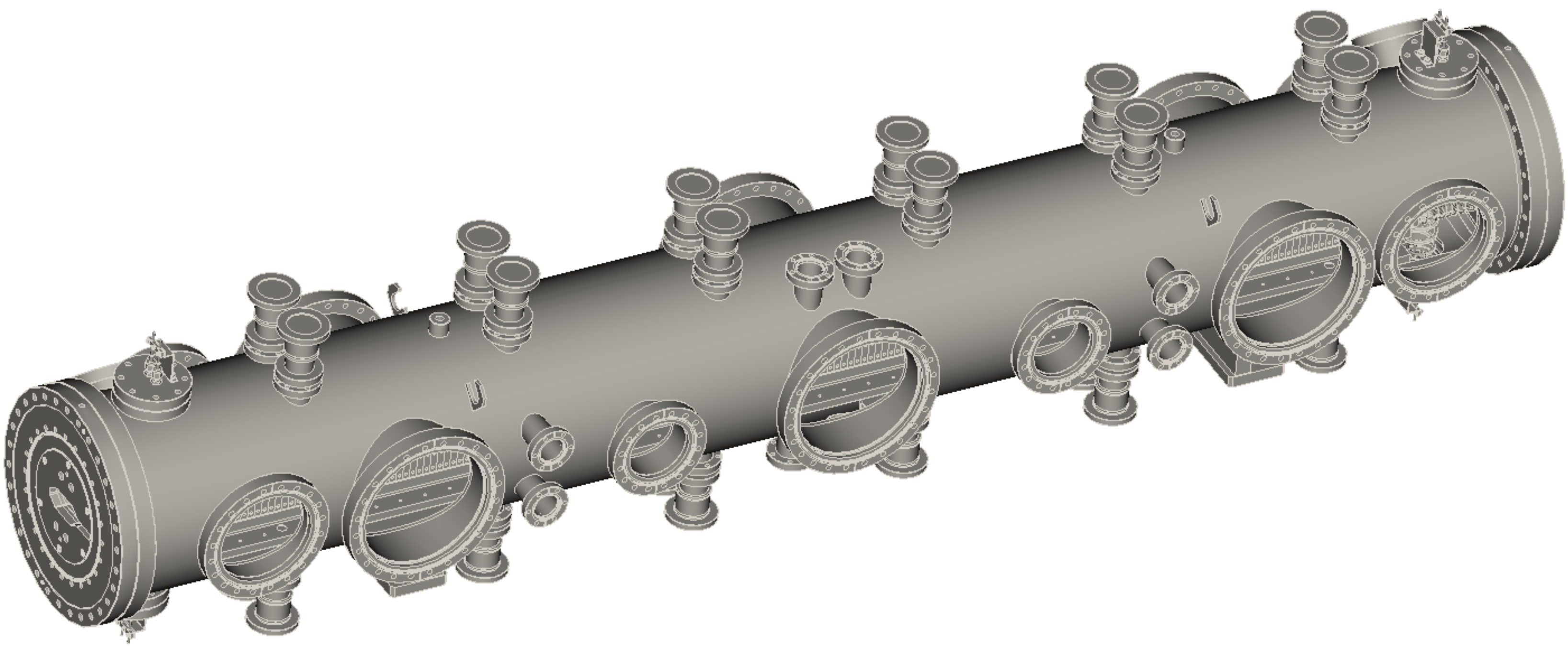

In-vacuum undulator, multi-bunch instabilities Beam based : Grow-damp measurement

K. Tian et al.
SLAC

- **Beam condition**
  - 500mA uniform filled beam in all buckets
  - Vertical chromaticity = 0
- **Grow-damp measurement**
  - Varying BL15 ID gap at 10um/step
  - Exponential fits of the amplitude growth of the dominating mode
  - Two series of instabilities are found
- **Trapped RF modes in the chamber**
  - Two modes induce 2 series of instability modes
  - RF modes frequency = beam instability mode frequency?

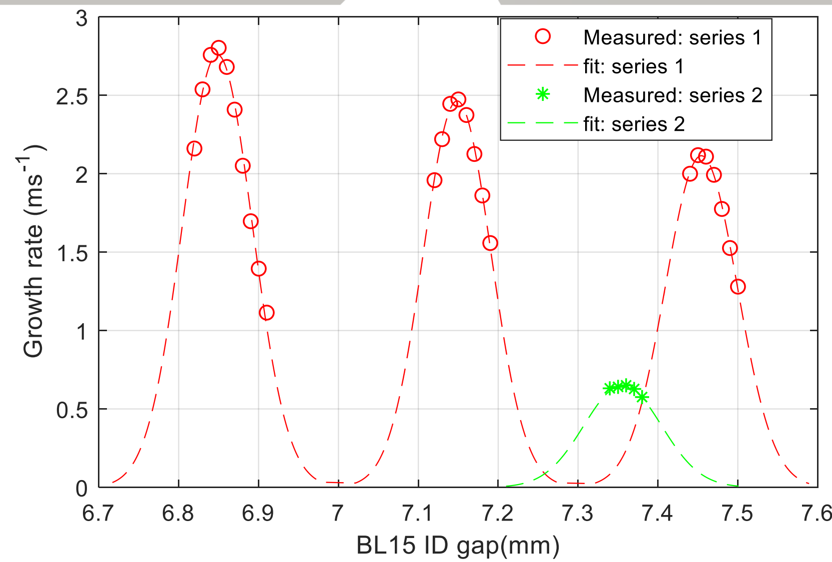

Gap (mm)	Mode index	Mode frequency (MHz)	BW (μm)	Q
6.85	156	199.51	72.9	641
7.15	157	200.79	70.6	666
7.45	158	202.07	75.0	631
7.36	118	150.86	81	NA

Gap=6.85mm, Evolution of Modes

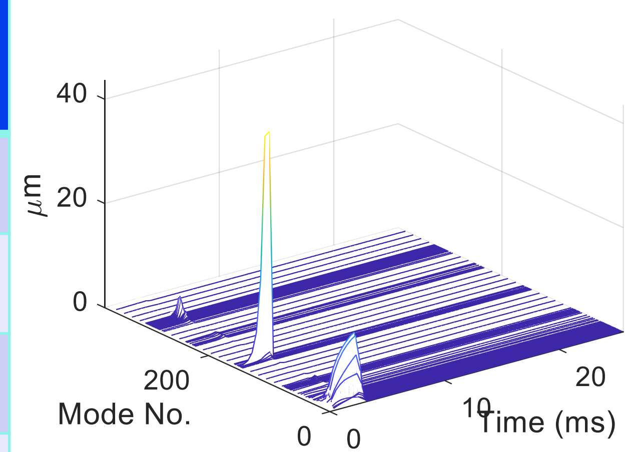

SPEAR3 BL15 IVU Chamber

K. Tian et al.

- IVU contains complex structures
  - Cooling tubes, flexible transitions, permanent magnet arrays,Al I-beam, bellows linked rods, thin metal sheets …
- Ridge wave guide like structure
  - Cut off frequency of a ridge wave guide decreases with the gap
  - The IVU chamber can support low frequency modes

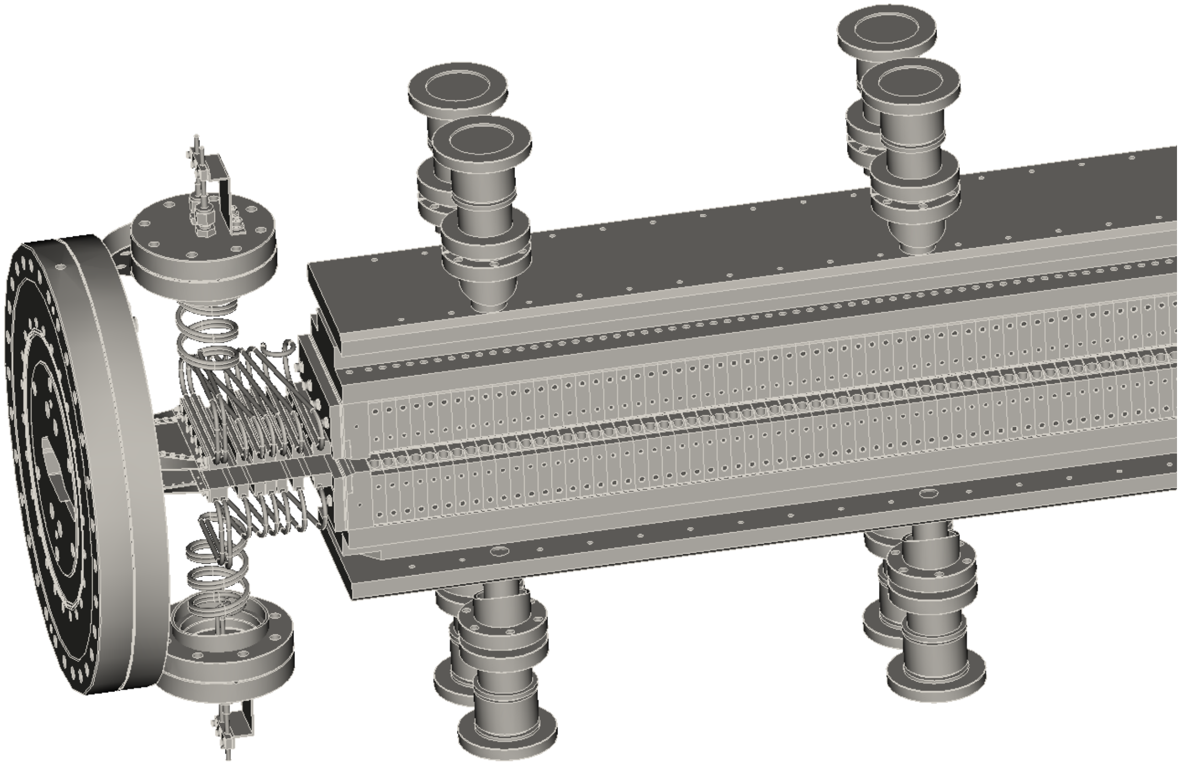

ID Cross Section

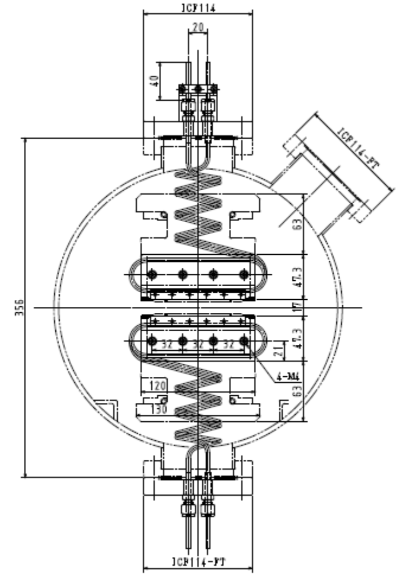

Ridge Waveguide

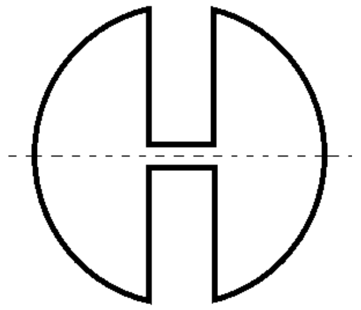

Simulation Results
Field Distribution of Mode #3

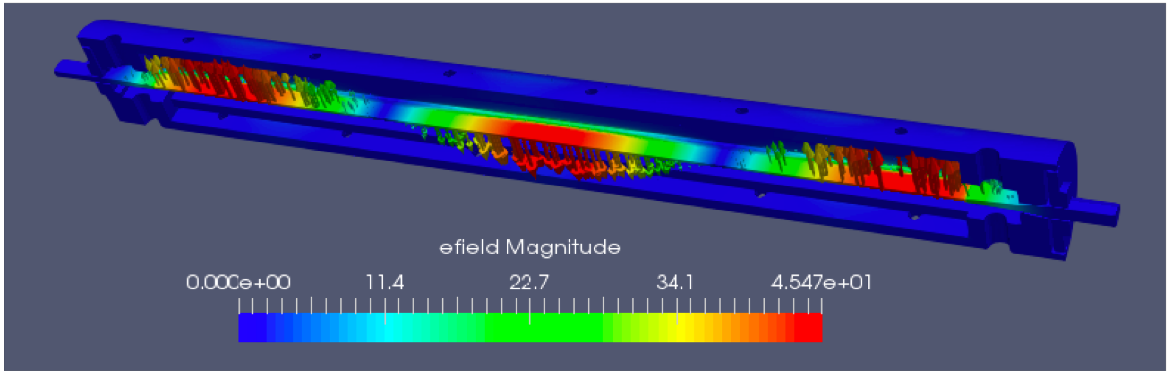

E field top view

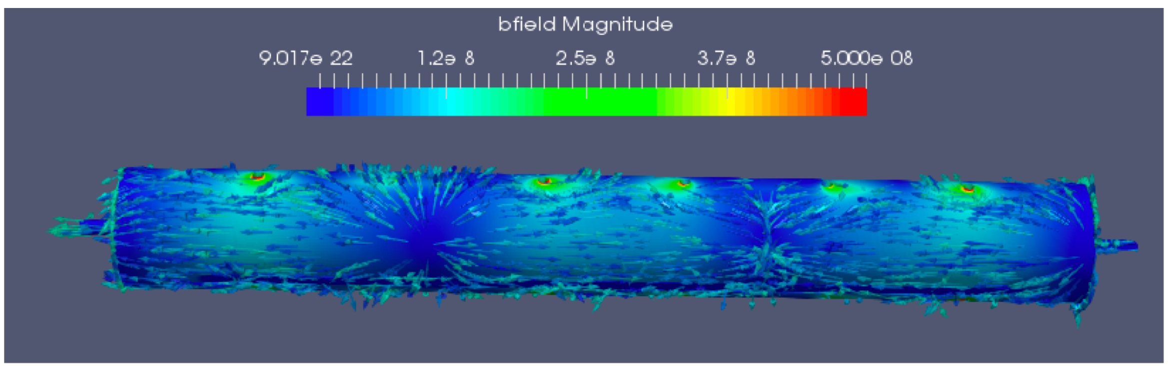

B field side view

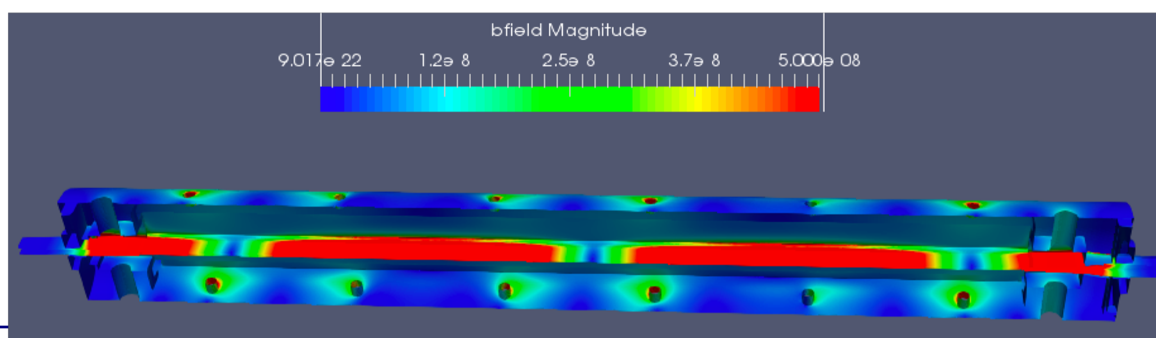

B field top view Note I-beam supports

S21 measurement with 2 antennas (no e-beam)

Single loop antenna

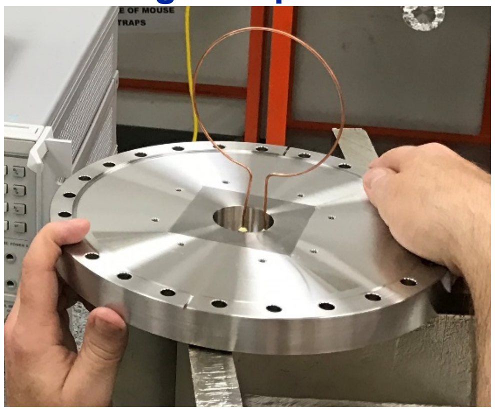

- Two single loop antennas were installed in port 1 and 2
  - Loop size is chosen as large as possible
- Three modes were found below 200MHz.

Port 2

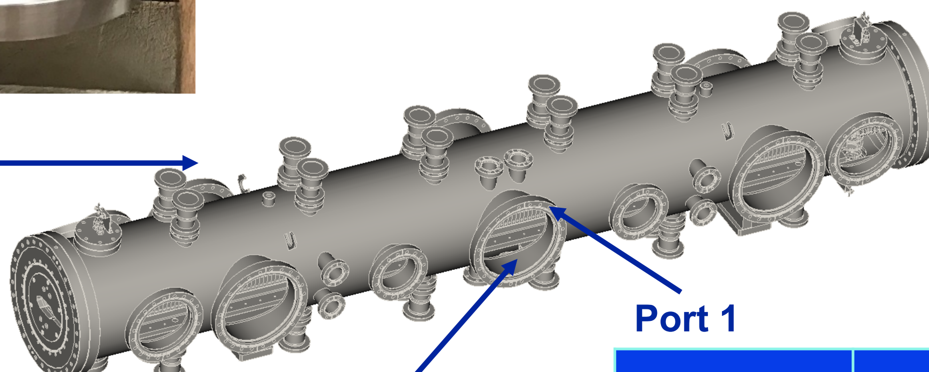

Port 1

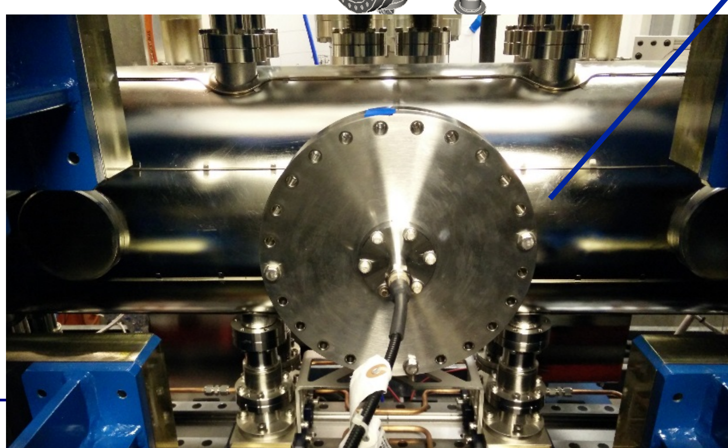

S21 Results (pole gap 6.82mm)

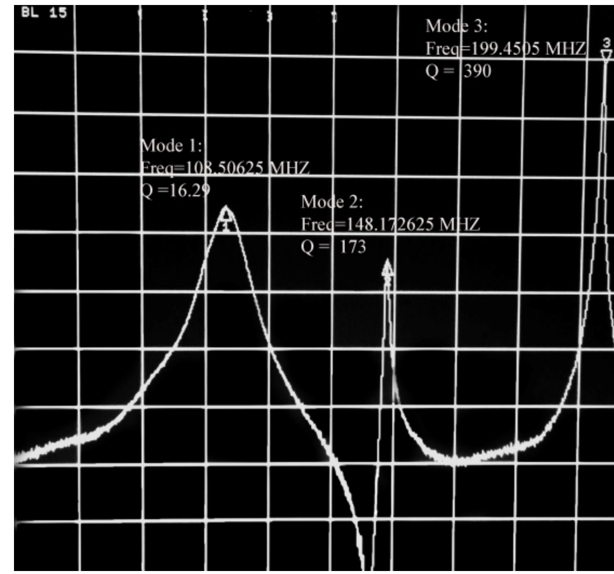

Mode #	f_{meas} (MHz)	Q_L (meas.)
1	108.5	16
2	148.17	173
3	199.45	390

Simulation Results Comparing with S21 measurement

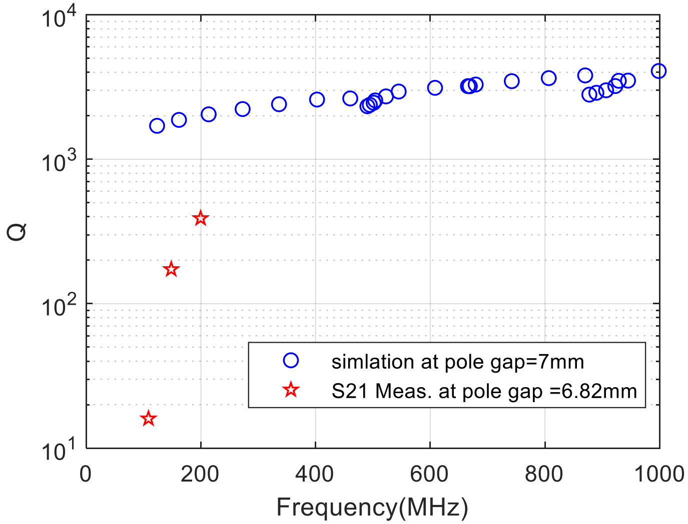

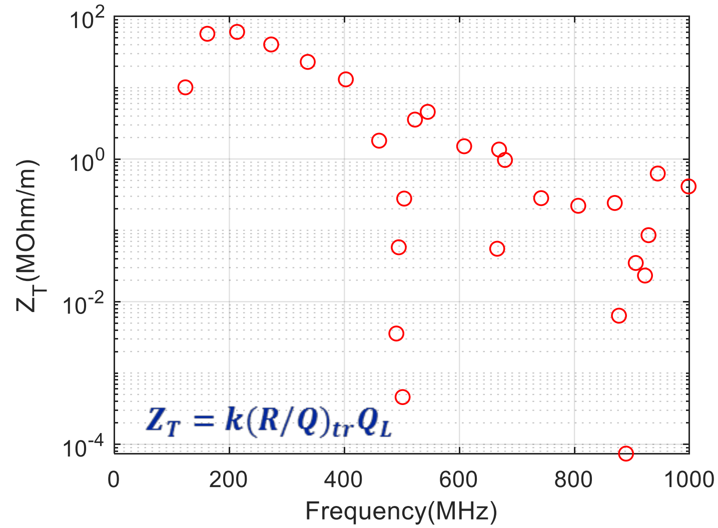

- **IVU pole gap settings are slightly different between simulation and S21 Measurement : 7mm vs 6.82mm**
- **Modes #1,2,3 can be identified in the simulation but with some discrepancies.**
- **Mode frequencies: good agreement; ~10% difference**
- **Quality factors: large difference; 1-2 orders of magnitude**
  - **Q_0 in simulation and Q_L in S21 measurement**
  - **Q_0 depends on the power loss on the surface and can be reduced by a factor of 2-3 by adding more geometric features into the simulation model and more tedious efforts in setting up surface materials**
  - **The reason for the large damping of mode #1 is unknown**
- **Transverse impedance Z_T**
  - **Modes #2 and #3 stand out**
  - **Absolute values are not accurate due to the uncertainty of Q_L**
  - **Impedance variation for different modes are due to geometric factors**

Approaches of passive damping

- Ferrite dampers : reduce Q_L ---- Choice of SPEAR3, installed in BL17 ID

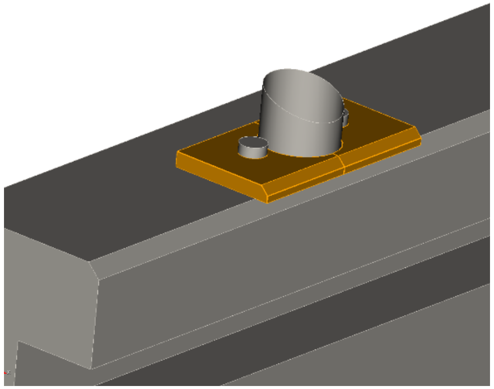

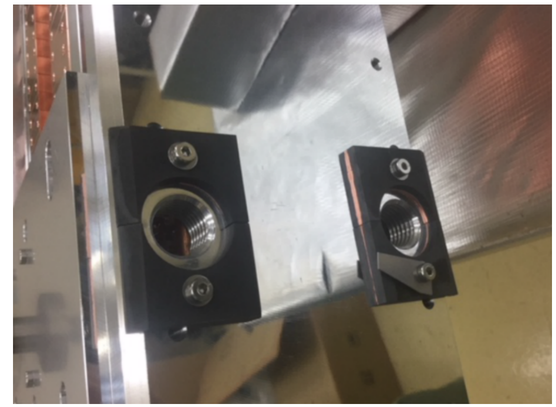

- Mode curtains : increase k and reduce $(R/Q)_{tr}$ ---- can work in some machines, but, for technical reasons, probably not in SPEAR3

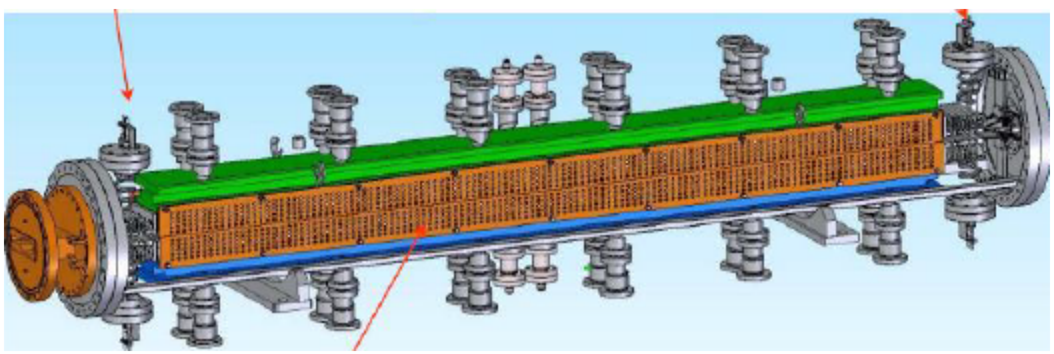

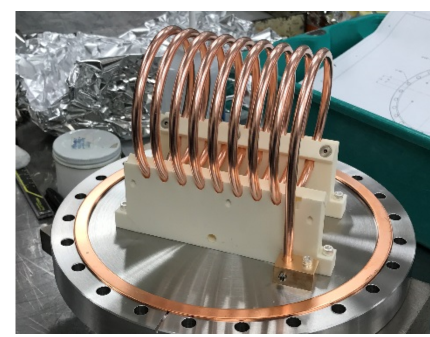

- Multi-turn loop antenna: reduce Q_L ---- not enough studies

Simulation Results
Damping performance and tolerance check

SLAC

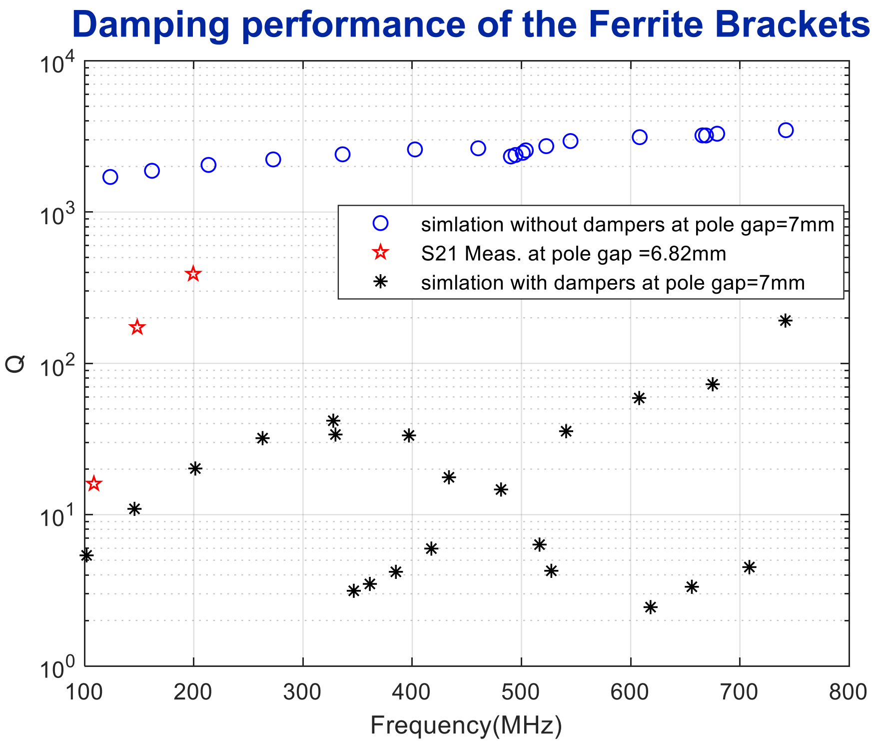

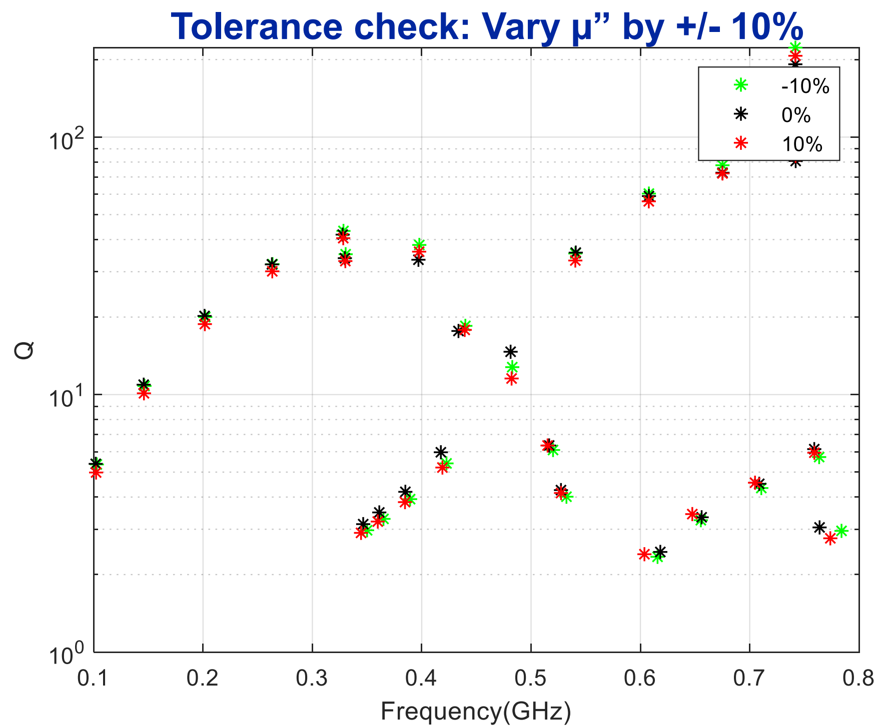

- Great damping performance across all frequency range
  - > two orders of magnitude from simulation results of bare ID
  - > one order of magnitude from S21 cold-test measurements of bare ID
- Tolerance check on the ferrite material properties
  - Vary ε’,ε”,μ’,μ”, each by +/-10%
  - No dramatic effects on the results
- Some convergence tests of meshing were also carried out

Simulation Results
Compare with BL17 ID S21 measurement

Neomax was able to include our design of the ferrite brackets into the new BL17 ID

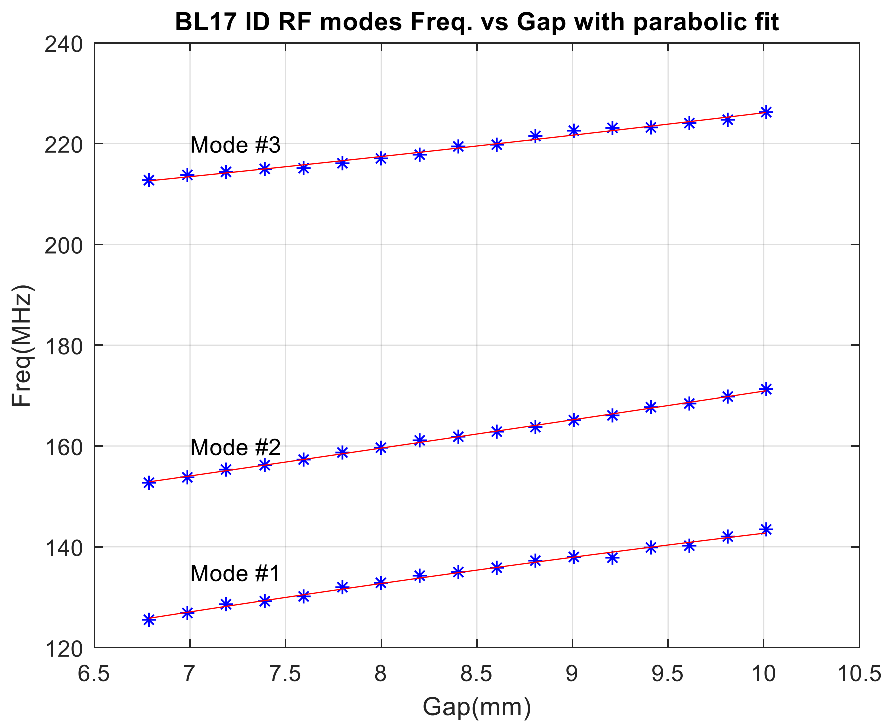

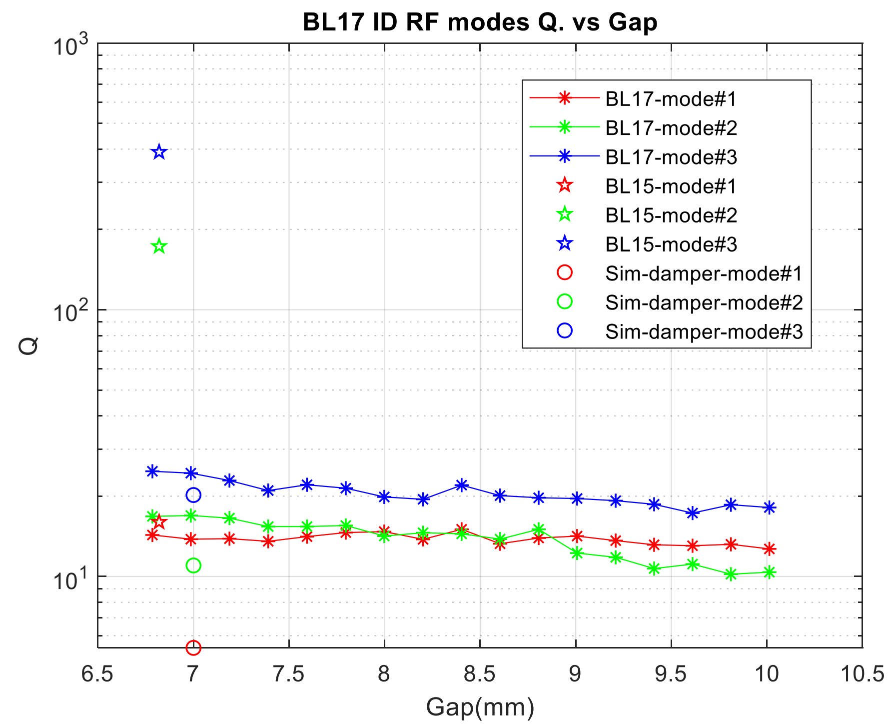

- **BL17 ID measurement**
  - Same cold test setup as with the BL15 ID S21 measurement
  - Measure mode frequencies and Qs at every 0.2 mm during pole gap scan
  - Observe the same three trapped modes at roughly the same frequencies
  - Compared with BL15 ID, modes #2 and #3 are damped by > 1 order of magnitude, roughly agree with simulation results (24 pairs of ferrites in design; 22 pairs actually installed)

Selected further reading

In-Vacuum undulator RF modes & multi-bunch instabilities

Kai Tian, Impedance studies on in-vacuum undulators, the 6th DLSR workshop, Berkeley, 2018

Modeling wigglers:

Weishi Wan, PAC03.

David Sagan, PAC03.

Ying Wu, PAC01 and PAC03.

Elleaume, Pascal, "A new approach to the electron beam dynamics in undulators and wiggler", EPAC'92, page 661.

Smith, Lloyd, "Effect of wigglers and undulators on beam dynamics", LBNL, ESG Technical Note No. 24, 1986.

EPU shims: J. Chavanne et al., "Recent achievements and future prospect of ID activities at the ESRF", EPAC2000.

Beam-based measurements:

Kuske, "Effects of fringe fields and insertion devices revealed through experimental frequency map analysis", PAC05.

Temnykh, "CESR-C: Performance of a wiggler-dominated storage ring", PAC05

Temnykh et al., "Beam based characterization of a new 7-pole superconducting wiggler at CESR", PAC05

Steier et al, "Study of row phase dependent skew quadrupole fields in apple-II type EPUs at the ALS", EPAC2004.

Temnykh et al., "Beam-based characterization of a new 7-pole super-conducting wiggler at CESR", PAC03.

Kuske et al., "Investigation of non-linear beam dynamics with apple II-type undulators at Bessy II", PAC01.

J. Safranek et al., "Nonlinear dynamics in a SPEAR wiggler", PRST-AB, Volume 5, (2002).

Robin et al., "Global beta-beating compensation of the ALS W16 wiggler", PAC97.

Orbit control:

O. Singh and S. Krinsky, "Orbit compensation for the time-varying elliptically polarized wiggler with switching frequency at 100 Hz.", PAC97.

Synchrotron Radiation simulation code:

Radiation2D: T. Shintake, http://www-xfel.spring8.or.jp/